FORMATION OF SOLAR PROMINENCES

P. K. Raju

Prepared under Grant NASA NsG 176-61

TABLE OF CONTENTS

ACKNOWLEDGEMENTS

I am indebted to my advisor, Professor L. Oster, for his help in every phase of the work. I wish also to thank Professor J. H. Hunter, who suggested this problem to me, for his guidance during the investigation.

Mrs. H. Miller and Miss J. Smith helped with the computer programming.

ABSTRACT

A non-linear treatment of prominence condensation from the corona by means of thermal instability is presented. It is found that the prominence stage is reached after times of the order 10^6 seconds. The major limitations on the process are due to magnetic fields; if the initial field strength is below 10^{-4} gauss, heat conduction by free electrons prevents the formation of condensations. On the other hand, fields above 10^{-1} gauss prohibit a significant density increase. It is suggested that the observed density values develop from secondary processes, after the temperature has reached prominence values as a result of initial thermal instability.

1. INTRODUCTION

Quiescent prominences pose two basic problems. One is their presumed origin out of the surrounding hot dilute corona. The second problem is their stability over long periods of time. We shall attempt to specify the physical conditions leading to the formation of prominence in this dissertation.

From stability studies, two major effects emerged that are of particular importance for the understanding of the formation process. Firstly, as originally suggested by Zanstra (1955), a quiescent prominence is in equilibrium with the coronal surroundings at approximately the same gas pressure. Secondly as discussed in detail by Kippenhahn and Schlüter (1957), following earlier work by Menzel (1951), and Dungey (1953), magnetic fields are required to hold the heavy prominence material up against gravitational forces. Both effects combined now mean that in a simplified model with essentially homogeneous magnetic fields the gravitational forces are balanced across the magnetic field lines, while at the same time pressure equilibrium is maintained and matter flow prohibited in this radial direction. The details of this thermal equilibrium as applied to fine structure elements within a quiescent prominence were discussed by Orrall and Zirker (1961), assuming vanishing optical thickness for each element, and most recently by Doherty and Menzel (1965) who included an approximate treatment of radiative transfer in the resonance lines of H, He I and He II to account for the chromospheric and coronal radiation field. They succeeded in obtaining models with

central kinetic temperatures lower than Orrall and Zirker's 30,000 ^{o}K. We conclude that a condensation process that permits to reach kinetic temperatures as low as 40,000 ^{o}K has effectively produced a prominence.

Discussions of thermal instability in connection with prominence formation were carried out by Kiepenheuer (1953a, 1953b, 1959), Parker (1953), Kleczek (1957, 1958), and Lüst and Zirin (1960). Weyman (1960b) derived the correct instability criterium for a compressible medium. Field (1965) then investigated the general concept of thermal instability in great detail for a wide variety of dilute gases, carrying out the perturbation analysis in the linear approximation. A similar investigation concentrating on the wave modes was carried out by Hunter (1966). Uchida (1963), on the other hand, extended the discussion to non-linear terms in an attempt to specify the triggering mechanism for the condensation which he identified with a cosmic ray stream generated during a flare at a neutral point of the magnetic field region. This model, due to the strict relation with flare events seems most suited for prominence situated in the areas of extreme field strengths near sunspots, in particular, for loop prominences. Quiescent prominences with their predominant occurrence outside of the spot region proper, are unlikely to be triggered in this manner. We shall come back to this point after discussion of the condensation process is completed.

This discussion is based on the set of hydromagnetic equations outlined in section 2, with the appropriate gain and loss functions derived in sections 3 and 4. The linear analysis is reviewed in

section 5, the non-linear treatment in section 6. Section 7, finally, contains a summary of the conclusions.

A survey of the historical development of prominence research and a brief list of facts of relevance to the study presented in this dissertation are given in Appendices.

2. FUNDAMENTAL EQUATIONS

Let the corona be represented by a uniform, dilute, gaseous medium in thermal and mechanical equilibrium. Since the corona is highly ionized, it behaves practically like a perfect conductor. In the absence of a magnetic field, or parallel to the force lines of a homogeneous magnetic field, heat conduction by free electrons would almost instantaneously dampen out any temperature inhomogeneity, as has been discussed, for instance, by Oster and Sofia (1966). Thus, the conjectured condensation of prominences out of the coronal material must take place across magnetic field lines, and a uniform magnetic field is presumed to be present throughout the corona. Along the field lines, no significant temperature gradient is expected. In praxi, the problem is of course much more complex in that the actual magnetic fields are highly inhomogeneous and, in the case of prominences, may be thought of as magnetic bottles. For our purposes, however, the assumption of a uniform field is sufficient and effectively reduces the problem to a one dimensional one.

The basic equations to be set down below then refer to motions across the magnetic lines of force. Due to the extreme tenuity of the corona, a magnetic field of the order of one gauss would already dominate the dynamics of the medium, instead of the internal gas pressure. We know that under coronal conditions, the mean free path for electrons and protons is a few thousand kilometers, a length which is of the order of prominence dimensions. Our equations now will use the continuum picture. In order to accept

this basis for the formation of a prominence, we must have scale lengths for the phenomenon that contain many mean free paths. In the presence of a magnetic field the mean free path is effectively replaced by the gyration radius as the relevant characteristic length. Computation shows that even at as low a field as 10^{-3} gauss and an electron temperature of 10^6 ^oK, the gyration radius for electrons is less than a kilometer, while for heavy ions it is around 10 km. The above argument then justifies our use of the continuum picture wherein the prominence is assumed to condense out of the corona across the field lines.

In the following, we review briefly the basic equations. Gaussian units are used throughout.

CONSERVATION OF MOMENTUM:

$$\rho \frac{d\vec{V}}{dt} = - \vec{\nabla} p_g + \frac{\vec{j} \times \vec{B}}{c} \quad . \tag{2.1}$$

Here, ρ is the gas density, p_g the gas pressure, $\vec{j}$ the electric current density, $\vec{B}$ the magnetic field strength, c the speed of light, and $\vec{V}$ the mass velocity.

CONSERVATION OF MASS:

$$\frac{d\rho}{dt} + \rho \, \vec{\nabla} \cdot \vec{V} = 0 \quad . \tag{2.2}$$

MAXWELL'S EQUATIONS:

$$\text{Curl } \vec{B} = 4\pi\vec{j}/c \tag{2.3}$$

$$\frac{1}{c} \frac{\partial \vec{B}}{\partial t} = - \text{ curl } \vec{\mathcal{E}} \quad , \tag{2.4}$$

$$\vec{\mathcal{E}} + \frac{\vec{V} \times \vec{B}}{c} = 0 \quad . \tag{2.5}$$

In equation (2.3), we have ignored the displacement current, as we are considering low frequency disturbances only. Equation (2.5) is the "frozen-field condition" on account of the magnetic flux conservation in a highly conducting fluid. In cases where large scale lengths are involved, this condition implies that the electric current is governed by the inductance of the medium rather than by resistivity, as is the case for prominences.

CONSERVATION OF ENERGY:

The law of energy conservation states in the present instance that the time rate of change of the total energy, stored within the fixed volume v and consisting of kinetic, internal, and electromagnetic energy, must equal the sum of the following terms: the rate of work done by mechanical forces acting on the fluid within the surface s, the influx of kinetic plus internal energy transported across the boundary, and the influx of heat and electromagnetic energy across the surface s. Expressed in integral form the law reads:

$$\frac{\partial}{\partial t}\int_v \left[\frac{1}{2}\rho V^2 + \rho U + \frac{B^2}{8\pi}\right] dv = -\int_s p_g \vec{V}\cdot d\vec{s}$$

$$-\int_s \left(\frac{1}{2}\rho V^2 + \rho U\right)\vec{V}\cdot d\vec{s} - \int_s (\vec{q} + \vec{s})\cdot d\vec{s} \quad . \qquad (2.6)$$

U is the intrinsic internal energy of the fluid, $\vec{q}$ the heat flow vector, $\vec{s}$ the electromagnetic flow vector equal to $c\vec{\mathcal{E}} \times \vec{B}/4\pi$. In the integral on the left-hand side we ignored the electrostatic term, as we had neglected the displacement current earlier. After simple algebraic manipulations and using the other conservation

equations along with Maxwell's equations, we get the following differential form for the law of energy conservation,

$$\rho \frac{dU}{dt} + p_g \vec{\nabla}\cdot\vec{V} = - \vec{\nabla}\cdot\vec{q} \quad . \tag{2.7}$$

At this stage we introduce the perfect gas law for the equation of state, viz.,

$$p_g = (\gamma - 1)C_v \rho T = (\gamma - 1)\rho U \ . \tag{2.8}$$

γ is the adiabatic coefficient, which is assumed constant, as over the range of temperatures to be considered no significant change in overall ionization is expected to occur. C_v is the specific heat at constant volume. Eliminating U between equations (2.7) and (2.8) we find

$$\frac{dp_g}{dt} = \frac{\gamma p_g}{\rho} \frac{d\rho}{dt} + (\gamma - 1)[-\vec{\nabla}\cdot\vec{q}]. \tag{2.9}$$

We split the divergence of the heat flux $\vec{\nabla}\cdot\vec{q}$ into two components. One is due to the heat conduction, the other due to the difference E-H between energy lost by radiation and gained by external sources (radiation, wave dissipation, corpuscular heating, etc.). The energy law then takes the following final form:

$$\vec{\nabla}\cdot\vec{q} = - \vec{\nabla}\cdot(K_B \vec{\nabla} T_e) + E - H \ , \tag{2.10}$$

and

$$\frac{dp_g}{dt} = \frac{\gamma p_g}{\rho} \frac{d\rho}{dt} + (\gamma - 1)[H - E + \vec{\nabla}\cdot(K_B \vec{\nabla} T_e)] \ . \tag{2.11}$$

One arrives at the same expression given by equation (2.11), incidentally, by taking the moments of the Boltzmann equation. K_B is the coefficient of thermal conductivity in the presence of a magnetic field. E is the "cooling function" for the radiation loss and H is the "heating function" due to external sources; both these functions will be specified later in detail. Note that on neglecting thermal conduction the magnetic field does not enter explicitly into the energy equation in the above form. This fact was overlooked by Uchida (1963).

K_B is given by Orrall and Zirker (1961), viz.,

$$K_B = 6 \times 10^{-17} \varphi^2 B^{-2} T_e^{-5/2} \qquad (2.12)$$

where T_e is the kinetic temperature of the electrons, φ equals $N_e T_e$, and N_e is the electron density.

In addition to the above basic equations, there is a very useful relation that can be obtained from the conservation equation of mass and magnetic flux:

$$B/\rho = \text{constant} . \qquad (2.13)$$

In particular, during the process of condensation from coronal to prominence conditions, we have

$$B_{\text{corona}}/\rho_{\text{corona}} = B_\ell/\rho_\ell \qquad (2.14)$$

where B_ℓ and ρ_ℓ are the values at any later stage.

3. COOLING FUNCTION

We define the "cooling function" as loss of internal energy by a unit volume per second. The internal energy of a volume element is identified with the kinetic energy of the free particles, since in our temperature and density range ionization and excitation energy can be neglected. Some of the kinetic energy of the particles is converted into radiation. If the medium is optically thin, all radiation counts toward the loss of internal energy. We will justify this assumption at a later stage in the discussion.

One loss mechanism is bremsstrahlung. Collisional excitation of atoms and ions to higher levels and the continuum accounts for another mechanism. In both cases, the electrons form the ultimate energy reservoir. The ions, then, via elastic collisions impart their kinetic energy to the electron gas and help reach a new velocity distribution at a lower kinetic temperature. Maxwellian distributions are assumed throughout.

The three loss mechanisms are thus:

1. Free-Free Emission,
2. Line Emission,
3. Free-Bound Emission.

The functional form of the free-free (bremsstrahlung) emission is (Orrall and Zirker (1961)),

$$E_{f-f} = 1.42 \times 10^{-27} N_e^2 T_e^{1/2} \text{ ergs cm}^{-3} \text{ sec}^{-1}. \qquad (3.1)$$

Here N_e is the electron density, T_e the electron temperature.

The line emission can be separated into two parts: permitted and forbidden line emission. Permitted line emission is always present. However, under certain conditions of temperature and density, forbidden line emission must be considered. This is the case in the corona. In our calculation we included this contribution for electron temperatures $\geq 10^5$ °K, and electron densities $\leq 10^9$. Orrall and Zirker (1961) found for the net forbidden line emission,

$$E_{f-L} = 3 \times 10^{-24} N_e^2 \text{ ergs cm}^{-3} \text{ sec}^{-1}. \qquad (3.2)$$

Let us now turn to permitted line and free-bound emissions. In both types of processes, an electron excites an ion from a lower bound level to a higher bound or to a continuum level. In steady state, and if the gas is optically thin, these upward transitions equal the downward radiative transitions. In computing the cooling by line and free-bound emissions we need to know the density of each ion or atom operative at a given temperature and electron density. To obtain this information it suffices to consider the statistical equation of state for transitions between the ground state and the continuum level only. Below 40,000 °K, these assumptions break down, but then we can say that a prominence has evolved.

We should like to discuss at this point, in some detail, the conceptual and computational limitations of the procedures adopted below for obtaining the actual radiative cooling rates.

Firstly, following Pottasch (1965), Doherty and Menzel (1965), and others, we restrict our considerations of line emissions to

the resonance lines, that under the physical conditions envisaged here lie in the near and far ultraviolet. This restriction is certainly permissible in the case of atoms such as H, He, and the higher stages of C, N, O, etc., whose excited bound levels are relatively high above the ground state. At the same time, in these atoms the assumption of a balance between collisional excitation and radiative deactivation will be an acceptable simplification. In support of this contention we made in Appendix B an estimate of the relative importance of emission in subordinate lines of metals, the hydrogen and helium subordinate lines, and the Balmer and Paschen continua. The outcome clearly shows that of all these features the Balmer lines are still the dominant source of radiation. It is fair to conclude therefore that the corresponding resonance lines will carry even more weight. Consequently, subordinate lines as well as metal free-bound continua are left out of our radiative cooling functions; this restriction, incidentally, is inherent as well in all previous work.

Secondly, the resonance lines which were considered were not corrected for finite optical depth. A decision as to the significance of this assumption is hard to make a priori, if only for the reason, that in reality an established prominence consists of a filamentary network of small dimensions whose elements or fine structures may well be optically thin in the metal resonance lines, while a computation of the optical depth for the overall dimension of a quiescent prominence would yield a rather large value. We feel that in the framework of the present investigation the assumption of negligible optical depth does not invalidate our

conclusions, although possibly the characteristic times and similar numerical quantities may be somewhat underestimated. It should be mentioned that in resonance lines the physical processes are complicated by scattering that prevents establishing the conditions of true absorption even for optical depths above unity; c.f. Ivanov-Holodnyi and Nikolskij (1961). Again we follow Pottasch in this respect.

We have computed the radiative loss of an optically thin element in the resonance lines of importance anew for two reasons: Firstly, the most recent similar work by Pottasch, and Doherty and Menzel give significantly different numerical results, with the origin of the difference being hard to determine from published data. Secondly, we wanted to include a few more elements than considered by Pottasch in order to be sure that no major source of cooling was left out. This applies, in particular, to N, S, and Fe. Altogether we considered H, He, C, N, O, Mg, Ne, Si, S, Fe. They are, according to Aller (1963) the ten most frequent elements in the solar plasma. Numerical values for their abundances are collected in Table 1, and compared with the values adopted by Pottasch.

Pottasch's expression for the emission rate in collisionally excited resonance lines reads

$$E_{a,\varepsilon} = Q_{exc} N_e N_{a,\varepsilon} \chi_{exc,erg} \text{ ergs cm}^{-3} \text{ sec}^{-1} \qquad (3.3)$$

where Q_{exc} is the collisional excitation rate, $\chi_{exc,erg}$ is the excitation energy in ergs, $\chi_{exc,ev}$ the same energy in eV. $N_{a,\varepsilon}$ is the ionic density for a particular element. The collision

rate Q_{exc} is given by Pottasch (1965) as

$$Q_{exc} = 1.70\times10^{-3}\ (gf_{iu})P(X_{exc})\chi_{exc,ev}^{-1}T_e^{-1/2}[\exp(X_{exc})]^{-1}. \quad (3.4)$$

(gf_{iu}) is the oscillator strength for the resonance multiplet. $P(X_{exc})$ is a numerical correction factor,

$$X_{exc} = 1.16 \times 10^4\ \chi_{exc,ev} \times T_e^{-1}\ . \quad (3.5)$$

Using equation (3.4) in equation (3.3), we get for the energy loss,

$$E_{a,\varepsilon} = 2.72\times10^{-15}(N_\varepsilon/N_H)(N_a/N_\varepsilon)N_e^2(N_H/N_e)(gf_{iu})P(X_{exc})^{-1/2}T_e[\exp(X_{exc})]^{-1} \quad (3.6)$$

N_ε is the number density of the element in question. N_H is the hydrogen density. N_a/N_ε constitutes the relative ion density for a given ionization stage of element ε. N_ε/N_H is the relative abundance with respect to hydrogen. Considering the medium to be practically a hydrogen-helium plasma, we can set N_e/N_H equal to 1.16, and rewrite equation (3.6) as

$$E_{a,\varepsilon} = 23.50\times10^{-16}N_e^2(N_\varepsilon/N_H)(N_a/N_\varepsilon)(gf_{iu})P(X_{exc})T_e^{-1/2}[\exp(X_{exc})]^{-1}. \quad (3.7)$$

Expressing the electron density in units of 10^7 particles per cm^3 so that N_e is equal to $N_e' \times 10^7$, we finally have,

$$E_{a,\varepsilon} = 23.50\times(N_\varepsilon/N_H)(N_a/N_\varepsilon)(gf_{iu})P(X_{exc})T_e^{-1/2}[\exp(X_{exc})]^{-1}\ N_e'^2 \quad (3.8)$$

Equation (3.8) has to be summed over all ions present at a given temperature to yield the total emission in resonance lines. For this purpose, the ionization ratio was computed for a given element as a function of temperature for different stages of ionization. The expression used here is given by House (1963):

$$n_{i+1}/n_i = 5.847\times10^{15}(3.10Z_i^2 - 1.20Z_i - 0.90)n^{-1}Z_i^{-2}T_e^{-2}X_i^{-3}[\exp(X_i)]^{-1}\xi_i. \quad (3.9)$$

where X_i equals $\chi_{i,ev}\times1.16\times10^4/T_e$. n is the principal quantum number of the lower ion. $\chi_{i,ev}$ is the ionization potential of the lower ion in eV, ξ_i is the number of electrons in the outer shell of the lower ion, Z_i is the ionic charge after ionization.

Using equation (3.9), we obtained the absolute density for various ions. At any temperature we ignored those ions whose relative density was less than 10%. This allowed at certain temperatures the use of four stages of ionization for a given element. As mentioned, the abundance figures were taken from Aller (1963). The values of (gf_{iu}) for various resonance lines were obtained from the article by Varsavsky (1961). $P(X_{exc})$ values were tabulated by Allen (1963). Actually, in our case $P(X_{exc})$ lies on the average around 0.25, except for neutral hydrogen and neutral helium for which necessary corrections were made. We considered temperatures between 1.5×10^6 °K and 2.5×10^4 °K.

The contribution of various processes to the total cooling has been tabulated below in Table 2. For comparison, the results obtained by Pottasch, and by Doherty and Menzel are summarized in Tables 4 and 5. The total energy loss is given as a plot of

log $E/N_e'^2$ vs log T_e (Fig. 1), together with the results by Pottasch (1965), and Doherty and Menzel (1965). The agreement with Pottasch is quite good. The difference between our curve and Pottasch's curve at high temperatures might be due to the higher abundance of Mg used by Pottasch and our inclusion of N, S, and Fe. The difference between our curve and Doherty and Menzel's results might be due to the somewhat different cross section adopted by them (a modified form of Elwert's (1954) cross section). However, they have not specified the chemical composition used in their calculations.

Summarizing then, we feel that the radiative cooling function is known to sufficient accuracy for our purposes, and that any difficulty could only arise in connection with the basic assumptions enumerated at the beginning of our discussion of line radiation. These assumptions, however, appear sufficiently justified in the present context.

Chemical composition:

Table 1.

Aller (1963)	Pottasch (1965)
$N_{He} = 0.16\ N_H$	$= 0.10\ N_H$
$N_C = 3.98 \times 10^{-4}\ N_H$	$= 5.00 \times 10^{-4}\ N_H$
$N_N = 1.10 \times 10^{-4}\ N_H$	--
$N_O = 8.81 \times 10^{-4}\ N_H$	$= 1.00 \times 10^{-3}\ N_H$
$N_{Ne} = 5.01 \times 10^{-4}\ N_H$	$= 1.00 \times 10^{-4}\ N_H$
$N_{Mg} = 2.69 \times 10^{-5}\ N_H$	$= 1.00 \times 10^{-4}\ N_H$
$N_{Si} = 3.16 \times 10^{-5}\ N_H$	$= 1.00 \times 10^{-4}\ N_H$
$N_S = 2.00 \times 10^{-5}\ N_H$	--
$N_{Fe} = 8.91 \times 10^{-6}\ N_H$	--

Radiative cooling rate: Our results

Radiative energy loss in the table below has been expressed in units of 10^{-9} ergs per cm^3 per sec per $N_e'^2$.

$$N_e = N_e' \times 10^7$$

where N_e is the electron density.

Table 2.

T_e, Electron temperature in ^oK	$E/N_e'^2$ Metals	$E/N_e'^2$ He II	$E/N_e'^2$ He I	$E/N_e'^2$ H	$E/N_e'^2$ Free-Free	$E/N_e'^2$ Forbidden line	$E/N_e'^2$ Total
2×10^4	2.96	--	0.009	11.0	2.01×10^{-2}	--	14.0
3×10^4	9.13	0.002	0.252	5.26	2.47×10^{-2}	--	14.7
4×10^4	16.9	0.224	0.275	2.78	2.84×10^{-2}	--	20.2
5×10^4	28.4	2.20	0.178	1.57	3.18×10^{-2}	--	32.4
6×10^4	41.8	9.04	0.127	1.41	3.48×10^{-2}	--	52.4
8×10^4	54.1	23.5	0.033	1.27	4.02×10^{-2}	--	79.0
1×10^5	53.6	16.6	--	--	4.49×10^{-2}	0.30	70.6
2×10^5	45.9	2.90	--	--	6.35×10^{-2}	"	49.1
3×10^5	25.1	1.18	--	--	7.78×10^{-2}	"	26.6
4×10^5	13.4	0.607	--	--	8.97×10^{-2}	"	14.4
6×10^5	5.44	0.367	--	--	1.10×10^{-2}	"	6.22
8×10^5	3.66	--	--	--	1.27×10^{-1}	"	4.09
1×10^6	2.12	--	--	--	1.42×10^{-1}	"	2.57
1.5×10^6	1.27	--	--	--	1.75×10^{-1}	"	1.74

Radiative cooling rate: Data for the graph from our results.

Table 3.

T_e, Electron temperature in ^oK	Log T_e	$E/N_e'^2$ ergs $cm^{-3}sec^{-1}$	log $E/N_e'^2$
$2.0x10^4$	4.30	$14.0x10^{-9}$	-7.86
$3.0x10^4$	4.48	$14.7x10^{-9}$	-7.83
$4.0x10^4$	4.60	$20.2x10^{-9}$	-7.69
$5.0x10^4$	4.70	$32.4x10^{-9}$	-7.49
$6.0x10^4$	4.78	$52.4x10^{-9}$	-7.28
$8.0x10^4$	4.90	$79.0x10^{-9}$	-7.10
$1.0x10^5$	5.00	$70.6x10^{-9}$	-7.15
$2.0x10^5$	5.30	$49.1x10^{-9}$	-7.31
$3.0x10^5$	5.48	$26.6x10^{-9}$	-7.57
$4.0x10^5$	5.60	$14.4x10^{-9}$	-7.84
$6.0x10^5$	5.78	$6.22x10^{-9}$	-8.21
$8.0x10^5$	5.90	$4.09x10^{-9}$	-8.39
$1.0x10^6$	6.00	$2.57x10^{-9}$	-8.59
$1.5x10^6$	6.18	$1.74x10^{-9}$	-8.76

Radiative cooling rate: Pottasch's results.

Table 4.

T_e, Electron temperature in ^oK	Log T_e	$E/N_e'^2$ ergs cm^{-3} sec^{-1}	Log $E/N_e'^2$
2.0×10^4	4.30	9.90×10^{-9}	-8.00
2.5×10^4	4.40	6.80×10^{-9}	-8.17
4.0×10^4	4.60	1.80×10^{-8}	-7.75
6.5×10^4	4.81	5.70×10^{-8}	-7.24
8.0×10^4	4.90	6.50×10^{-8}	-7.19
1.0×10^5	5.00	5.00×10^{-8}	-7.30
1.25×10^5	5.10	5.70×10^{-8}	-7.25
1.6×10^5	5.20	5.70×10^{-8}	-7.25
2.0×10^5	5.30	6.50×10^{-8}	-7.19
3.0×10^5	5.48	3.20×10^{-8}	-7.50
4.0×10^5	5.60	1.70×10^{-8}	-7.77
6.5×10^5	5.81	1.20×10^{-8}	-7.92
8.0×10^5	5.90	9.30×10^{-9}	-8.03
1.0×10^6	6.00	7.50×10^{-9}	-8.13
2.0×10^6	6.30	4.40×10^{-9}	-8.36

Radiative cooling rate: Doherty and Menzel's results.

Table 5.

T_e, Electron temperature in ^oK	Log T_e	$E/N_e'^2$ ergs $cm^{-3}sec^{-1}$	log $E/N_e'^2$	Log E
$1.0x10^4$	4.00	$1.00x10^{-9}$	-9.00	-3.00
$1.8x10^4$	4.25	$4.37x10^{-9}$	-8.36	-2.86
$3.2x10^4$	4.50	$1.64x10^{-8}$	-7.79	-2.79
$5.6x10^4$	4.75	$8.51x10^{-8}$	-7.07	-2.57
$1.0x10^5$	5.00	$2.27x10^{-7}$	-6.64	-2.64
$1.8x10^5$	5.25	$3.16x10^{-7}$	-6.50	-3.00
$3.2x10^5$	5.50	$1.70x10^{-7}$	-6.77	-3.77
$5.6x10^5$	5.75	$4.26x10^{-8}$	-7.37	-4.87
$1.0x10^6$	6.00	$5.89x10^{-9}$	-8.23	-6.23
$1.5x10^6$	6.18	$1.95x10^{-9}$	-8.71	-7.02

4. HEATING FUNCTION

Let us now define the "heating function" entering equations (2.10) and (2.11). A volume element in the corona would remain in thermal equilibrium so long as it gains as much energy as it loses via radiation. There are several means of supplying heat energy, in particular,

1. Photoionization,
2. Wave dissipation,
3. Corpuscular heating.

Note that conduction was separated out in equations (2.10) and (2.11).

Photoionization, as we have stated earlier, is not important under coronal conditions. It would be significant at temperatures where prominences are stable. Above some 4×10^4 ^{o}K we need not worry about this contribution.

We are then left with contributions 2 and 3. In both these cases, the heat input would depend on the local density of the medium. This can be seen as follows: The energy of a wave resides in the translational energy of the particles subjected to wave motion at any given point. In order for the wave to dissipate its energy, it must transform this ordered kinetic energy into random kinetic energy of the surrounding medium. The transfer is the more effective the higher the number of particles is that are available for collisions. Thus, heat input by wave dissipation is proportional to the local density of the medium, as suggested, for instance, by Weyman (1960a), and quoted by Field (1965).

The same argument now holds for corpuscular heating. At this point it might be worth noting that the Sun is thought to generate a radial corpuscular stream of particles. During the passage through chromosphere and corona, the stream will lose some of its translational energy by heating the medium before it merges from the corona as the observed solar wind.

In our analysis we will use a heat input function, due to wave dissipation or corpuscular heating, in the form,

$$H = A_o \rho \ . \qquad (4.1)$$

where A_o is a constant to be specified later, ρ is the local matter density.

We are now ready to apply the basic equations developed in chapter 2 to the stability analysis. Chapter 5 is concerned with the linear analysis, whereas chapter 6 will be devoted to the non-linear treatment.

5. LINEAR OSCILLATIONS

In the present chapter we make use of the basic equations set up in chapter 2, together with the cooling and heating functions, as specified, to analyze the stability behavior of the solar corona. This problem has been discussed by Field (1965) in the general context of thermal instability. We briefly summarize the analysis, discussing in some detail those aspects of particular significance for our later non-linear treatment.

We consider the corona as a uniform, dilute gaseous medium behaving like a perfect conductor. A uniform magnetic field is supposed to be prevailing throughout the corona. In the undisturbed state the corona is in thermal and mechanical equilibrium. This state is characterized by the balance,

$$H_o - E_o = 0 \quad . \tag{5.1}$$

H_o is the heat input per cm^3 per second, E_o is the corresponding energy loss via radiation. Mechanical equilibrium for the initial state is preserved by the absence of any inhomogeneity in physical quantities. In the present chapter we want to study the thermal stability of the medium around equilibrium, when the medium is subjected to infinitesimal perturbations. The analysis amounts to obtaining the dispersion relation for linear hydromagnetic oscillations. The roots of the dispersion relation reveal the possible existence of any unstable thermal mode that will lead to condensation within the medium.

The linearized equations in the perturbed form read as follows:

MOMENTUM CONSERVATION

$$\rho_o \frac{\partial \vec{V}}{\partial t} = - \vec{\nabla} p + \frac{\vec{j} \times \vec{B}_o}{c} \quad . \tag{5.2}$$

MASS CONSERVATION

$$\frac{\partial \rho}{\partial t} = - \rho_o \vec{\nabla} \cdot \vec{V} \quad . \tag{5.3}$$

ENERGY CONSERVATION

$$\frac{\partial p}{\partial t} = \frac{\gamma p_o}{\rho_o} \frac{\partial \rho}{\partial t} + (\gamma - 1)\left[\left(\frac{\partial H_o}{\partial \rho_o} - \frac{\partial E_o}{\partial \rho_o}\right)\rho + \left(\frac{\partial H_o}{\partial T_o} - \frac{\partial E_o}{\partial T_o}\right)T + K_o \nabla^2 T\right]. \tag{5.4}$$

EQUATION OF STATE

$$p/p_o = \rho/\rho_o + T/T_o \quad . \tag{5.5}$$

MAXWELL'S EQUATIONS

$$\frac{1}{c} \frac{\partial \vec{h}}{\partial t} = - \text{curl } \vec{\mathcal{E}} \quad . \tag{5.6}$$

$$\mathcal{E} = - \frac{V \times B_o}{c} \tag{5.7}$$

From equations (5.6) and (5.7) we get,

$$\frac{\partial \vec{h}}{\partial t} = \text{curl } (\vec{V} \times \vec{B}_o) \quad . \tag{5.8}$$

Quantities with the subscripts 'o' are the unperturbed equilibrium values. All other quantities represent small departures from the equilibrium values. $\vec{h}$ is the perturbed magnetic field strength.

$\vec{j}$ is the induced electric current density. We specify the perturbation to have the wave form,

$$q_o e^{\omega t+ikx}$$

where q_o is the amplitude, k the wave number along the x-direction, and ω the frequency of the disturbance.

Eliminating all the perturbed physical variables from equations (5.2) - (5.8), we get the following expression for the dispersion equation,

$$(\omega^2 + k^2V_x'^2)\left[\omega^3 + \frac{(\gamma-1)}{p_o}\left\{K_oT_ok^2 + T_oL_T\right\}\omega^2 + k^2(V_z'^2+C_s^2)\omega\right.$$

$$\left. + \left(\frac{\gamma-1}{p_o}\right)k^2\left\{K_oT_ok^2(V_z'^2+ C_s^2/\gamma) + V_z'^2L_TT_o+C_s^2/\gamma\ [L_TT_o-L_\rho\rho_o]\right\}\right]$$

$$- V_x'^2V_z'^2k^4\left[\omega + \frac{\gamma-1}{p_o}(K_oT_ok^2+L_TT_o)\right] = 0 \ . \qquad (5.9)$$

where K_o is the equilibrium thermal conductivity coefficient in the presence of a magnetic field.

Furthermore, we have,

$$L_T = \left(\frac{\partial E_o}{\partial T_o} - \frac{\partial H_o}{\partial T_o}\right) , \qquad L_\rho = \left(\frac{\partial E_o}{\partial \rho_o} - \frac{\partial H_o}{\partial \rho_o}\right)$$

$$C_s = \sqrt{\gamma p_o/\rho_o} \quad \text{(sound speed)}, \quad V_x' = B_{ox}/\sqrt{4\pi\rho_o} \ ,$$

$$V_z' = B_{oz}/\sqrt{4\pi\rho_o} \quad \text{(Alfven speed)} \ .$$

The above dispersion equation is similar to the one obtained by Field (1965). The last bracketted term in equation (5.9) brings out the effect of oblique propagation. In order to study the maximum effect of magnetic field, we restrict ourselves to the case where the propagation vector is perpendicular to the magnetic field. We expect the prominence to condense out of the corona across the field lines, since in this manner conduction is inhibited, and the prominence is allowed to develop.

We let the x-component of the magnetic field equal to zero and let the field lines run normal to the x-y plane. The dispersion equation then takes the form,

$$\omega^3 + \frac{\gamma-1}{p_o}\left\{K_o T_o k^2 + T_o L_T\right\}\omega^2 + k^2(V_z'^2 + C_s^2)\omega$$

$$+ \frac{\gamma-1}{p_o} k^2\left\{K_o T_o k^2(V_z'^2 + \frac{C_s^2}{\gamma}) + V_z'^2 L_T T_o + \frac{C_s^2}{\gamma}(L_T T_o - L_\rho \rho_o)\right\} = 0. \tag{5.10}$$

Thus we have three modes of oscillations given by the three roots in ω. For a given k, instability would set in if equation (5.10) has one real positive root. The general condition for equation (5.10) to have at least one real positive root is to have the term independent of ω less than zero. Thus for thermal instability to occur we find the condition,

$$\frac{K_o T_o k^2}{E_o} + L_T \frac{T_o}{E_o} - \frac{\rho_o}{E_o} \frac{L_\rho}{1 + \gamma V_z'^2/C_s^2} < 0 . \tag{5.11}$$

The radiative cooling function, as seen from equation (3.7), is proportional to the square of the electron density and to some function of temperature, discussed in chapter 3, and given by Fig. 1. From the cooling curve it is clear that one could represent the temperature function by some power of T_e, with the temperature index defining the slope of the curve at any given temperature. As is obvious from the shape of the curve, the slope changes as a function of temperature.

We express the cooling function in the analytic form as

$$E_o = C_o \rho_o^2 T_e^{\beta} , \qquad (5.12)$$

where C_o is constant, β is temperature index, ρ_o is the equilibrium matter density. Using equations (4.1), (5.1), and (5.12) in equation (5.11) we get the instability criteria

$$\frac{K_o T_o k^2}{E_o} + \beta - \frac{1}{1 + \gamma V_z'^2 / C_s^2} \leq 0 . \qquad (5.13)$$

Equality in (5.13) represents the marginal case. On the positive side of equality we have all stable modes, on the negative side as displayed by (5.13), we have at least one unstable mode. The instability criterion given above is similar to the one obtained by Field for isobaric thermal modes. When $k^2 = E_o / K_o T_o = k_c^2$ conduction will balance the radiative losses, where the thermal conductivity as quoted in chapter 2, is given by,

$$K_o = 6 \times 10^{-17} \varphi^2 B_o^{-2} T_e^{-5/2} \quad \text{ergs cm}^{-1}\text{sec}^{-1}\text{deg}^{-1} ,$$

with

$$\varphi = N_e T_e \ .$$

We tabulate below a few equilibrium values, as an aid to the discussion of (5.13). For illustrative purposes, we use Doherty and Menzel's cooling curve to get the values of $\beta \cdot \varphi$ is assumed constant and $\gamma = 5/3$.

Constancy of φ implies that under isobaric conditions the equilibrium magnetic field may not be greater than 6×10^{-3} gauss. At higher magnetic field strengths, φ is not constant during the condensation process. In the extreme case, where the magnetic field dominates the pressure balance, and the plasma acts as an incompressible fluid, the density remains essentially constant and only the temperature drops. This behavior is verified by the non-linear analysis to follow.

On the other hand, our expression for the thermal conductivity, as reduced by the presence of a magnetic field, is valid for the complete condensation process, provided that the initial field is at least 1×10^{-4} gauss. We will come back to these points in detail in chapter 7.

From Table 6 we see that around 10^6 ^oK and for a field of 10^{-3} gauss thermal conduction can be ignored for wave numbers $k \leq 10^{-9}$ cm^{-1}. A more detailed justification for this neglect of thermal conduction is given in Appendix C.

Since $|\beta| > 1$, the corona becomes thermally unstable to small perturbations around the equilibrium. Moreover, the velocity of sound is high enough to insure isobaric perturbations, if the characteristic time for a prominence to evolve is greater than

Table of equilibrium values;

Table 6.

T_e, Electron temperature in ^oK	N_e in cm^{-3}	$p_g = 2N_e kT_e$ dynes cm^{-2}	C_s^2 cm^2/sec^2	C_s^2/V_z^2	E_o ergs $cm^{-3}sec^{-1}$	$\frac{K_o T_e k^2}{E_o}$	β
$1x10^6$	$2x10^8$	$5.5x10^{-2}$	$2.8x10^{14}$	$1.2xB^{-2}$	$5.1x10^{-7}$	$4.7x10^9 k^2 B_o^{-2}$	-3.6
$8x10^5$	$2.5x10^8$	"	$2.2x10^{14}$	"	$1.9x10^{-6}$	$1.8x10^9 k^2 B_o^{-2}$	-3.6
$5x10^5$	$4x10^8$	"	$1.4x10^{14}$	"	$2.7x10^{-5}$	$2.5x10^8 k^2 B_o^{-2}$	-2.6
$2x10^5$	$1x10^9$	"	$5.6x10^{13}$	"	$6.2x10^{-4}$	$4.4x10^7 k^2 B_o^{-2}$	-0.6

1000 seconds. This time of 1000 seconds is the time required by a sound pulse to traverse a distance of 100,000 km at the sound speed of 100 km per second. Thus, the observed life times for quiescent prominences indicate that their evolution indeed follows isobaric conditions. Neglecting thus thermal conduction, the instability criterion becomes

$$\beta - \frac{1}{1 + \gamma V_z'^2/c_s^2} < 0 \quad . \tag{5.14}$$

For our cooling function, β is less than zero for a considerable range of electron temperatures. When the magnetic pressure is small compared to the internal gas pressure, inequality (5.14) yields

$$-1 + \beta < 0 \quad , \tag{5.15}$$

whereas for magnetic pressures above the gas pressure, we have for thermal instability to occur:

$$\beta < 0 \quad . \tag{5.16}$$

This result is well known.

However, condition (5.16) in our case is rather puzzling. At the outset, it states that even at extremely large magnetic fields one could obtain condensations across the field lines, although with increasing field strength it becomes more and more difficult to compress conducting matter across the field lines, since the magnetic field has the property of imparting rigidity to the electrically conducting medium. The answer to the problem

is furnished by the mode amplitudes. Since our dispersion equation is of third degree, we have three modes of propagation. One of the modes is a pure thermal mode, the other two are compressional modes. In a linearized theory, the density fluctuations at any time and position may be represented as the algebraic sum of density fluctuations due to all the three modes. We then have

$$\rho(x,t) = A_k(x)\, e^{\omega_1 t} + B_k(x) e^{\omega_2 t} + C_k(x) e^{\omega_3 t} \,. \qquad (5.17)$$

A_k, B_k, and C_k are the mode amplitudes for the three modes of a given wave number k. The ω's are the respective frequencies furnished by the three roots of the dispersion equation. We can derive the mode amplitudes by specifying initial values of the perturbed quantities such as density, pressure, etc. Two more equations are needed to solve for the three unknowns A_k, B_k, and C_k. Since the set of basic equations can be transformed into a third order time dependent differential equation in density, the required two equations, in principle, are of the form

$$\frac{\partial}{\partial t}\rho(x,t)\Big|_{t=0} = \omega_1 A_k(x) + \omega_2 B_k(x) + \omega_3 C_k(x) \,, \qquad (5.18)$$

and

$$\frac{\partial^2 \rho(x,t)}{\partial t^2}\Big|_{t=0} = \omega_1^2 A_k(x) + \omega_2^2 B_k(x) + \omega_3^2 C_k(x) \,. \qquad (5.19)$$

Solving equations (5.17) - (5.19) simultaneously for A_k, B_k, and C_k, we get

$$A_k(x) = \frac{\delta + \alpha(W_o^2+W_1^2) - 2W_o\theta}{W^2-2WW_o+W_o^2+W_1^2} \quad \text{(Thermal mode)} \tag{5.20}$$

$$B_k = x + iy \,, \qquad C_k = x - iy \quad \text{(compressional mode)} \,. \tag{5.21}$$

Where,

$$\alpha = \rho(x,0) \,, \qquad \theta = \left.\frac{\partial\rho}{\partial t}(x,t)\right|_{t=0} = -\rho_o \frac{\partial V_x}{\partial x}$$

$$\delta = \left.\frac{\partial^2\rho}{\partial t^2}(x,t)\right|_{t=0} = V_z'^2 \frac{\partial^2\rho}{\partial x^2} + \frac{\partial^2 p}{\partial x^2} \,. \tag{5.22}$$

$$\omega_1 = W \,, \quad \omega_2 = W_o + iW_1 \,, \quad \omega_3 = W_o - iW_1$$

$$x = \frac{(\alpha W^2-\delta)+2W_o(\theta-\alpha W)}{2[W^2-2WW_o+W_o^2+W_1^2]} \tag{5.23}$$

$$y = \frac{(\theta-\alpha W)(W_o^2-W_1^2) + W_o(\alpha W^2-\delta) + W(\delta-\theta W)}{2W_1[W^2 - 2WW_o + W_o^2 + W_1^2]}$$

In order to specify the amplitudes, we must know W, W_o, and W_1, as function of the equilibrium values. This amounts to finding the roots of the dispersion equation (5.10). Ignoring thermal conduction, equation (5.10) can be written as

$$\omega^3 + \frac{(\gamma-1)E_o\beta\omega^2}{p_o} + k^2V_z'^2(1 + C_s^2/V_z'^2)\omega$$

$$+ \frac{\gamma-1}{p_o} E_o k^2 V_z'^2 (1 + C_s^2/\gamma V_z'^2)\left[\beta - \frac{C_s^2/\gamma V_z'^2}{1 + C_s^2/\gamma V_z'^2}\right] = 0 \qquad (5.24)$$

In our case when the magnetic pressure is large compared with the internal gas pressure, so that we can ignore $C_s^2/V_z'^2$ as compared to one, equation (5.24) for $|\beta| > 1$ becomes

$$\omega^3 + \frac{\gamma-1}{p_o} E_o \beta\omega^2 + k^2V_z'^2\omega + \frac{\gamma-1}{p_o} E_o k^2 V_z'^2 \beta = 0 \quad . \qquad (5.25)$$

Equation (5.25) has the following three roots:

$$\omega_1 = - \frac{(\gamma-1)E_o\beta}{p_o} \qquad \text{(Thermal mode)} \quad . \qquad (5.26)$$

$$\omega_{2,3} = \pm\, ikV_z' \qquad \text{(Compressional mode)} \quad . \qquad (5.27)$$

If $\beta < 0$, the thermal mode is unstable, otherwise it is stable. Referring to equation (5.22), we have in the case of high magnetic field the following roots for the dispersion equation,

$$W = - (\gamma-1)E_o\beta/p_o$$

$$W_o = 0 \ , \qquad W_1 = \pm\, kV_z' \quad . \qquad (5.28)$$

From equation (5.28), the mode amplitude for the thermal mode is found as

$$A_k = \frac{\delta + \alpha k^2 V_z'^2}{W^2 + k^2 V_z'^2} = \frac{V_z'^2 (k^2 + \frac{\partial^2 \rho}{\partial x^2}) + \frac{\partial^2 p(x,0)}{\partial x^2}}{W^2 + k^2 V_z'^2} \quad . \qquad (5.29)$$

For any arbitrary initial disturbance of density, which can be Fourier-analyzed into components, the terms containing the density function in the numerator of equation (5.29) cancel out to zero. The only place where we would have terms containing the magnetic field is in the denominator of equation (5.29). Thus the amplitude of the thermal mode is proportional to the inverse square of the magnetic field strength. This result simply means that unstable thermal modes, although possible in principle, would find it hard to develop across the lines of strong magnetic fields, so that at sufficient field strength we are left with the two compressional modes, travelling across the field lines at the Alfvén speed.

Before we turn to the non-linear analysis we have to ascertain that in the temperature range considered, equilibrium is not reached, i.e., that a stable configuration results only at temperatures below 4×10^4 ^oK which we take as an acceptable upper limit for the electron temperature in quiescent prominences.

For this purpose, we consider first the initial equilibrium state given by

$$C_o \rho_o^2 T_o^\beta = A_o \rho_o \quad .$$

Thus,

$$A_o = C_o \rho_o T_o^\beta \quad . \qquad (5.30)$$

In order that thermal equilibrium be attained at a later stage, we must have

$$A_o\rho = C_o\rho^2 T^\nu$$

or else

$$C_o\rho^2 T^\nu > A_o\rho \ . \qquad (5.31)$$

Upon replacing the value of A_o from equation (5.30) in equation (5.31) we find the inequality

$$(\rho/\rho_o)T^\nu/T_o^\beta > 1 \ .$$

If β is less than zero (which is true for the radiative cooling function over the whole range under consideration), then let $\beta = -\beta_o$ with $\beta_o > 0$. The inequality now reduces to

$$(\rho/\rho_o)T^\nu/T_o^{-\beta_o} > 1 \ .$$

Since ρ is greater than ρ_o, and $T_o > T$, the system will indeed not attain thermal equilibrium at any later stage.

However, we can suspect that, as the condensation process approaches the actual prominence temperature, radiation losses will diminish due to the decrease in the number of electrons. This drop in electron density is brought about by a decrease in overall ionization. Moreover, the prominence will become optically thick to chromospheric radiation, in particular, the resonance continua of H and He I which provide an additional, efficient heating mechanism.

Due to flux conservation, the magnetic field strength will increase under condensation. If at any intermediate stage the field becomes large enough to satisfy the inequality (5.16), further condensation across the field lines is effectively prohibited. This is indeed borne out by the non-linear analysis to be discussed presently.

6. NON-LINEAR CALCULATIONS

In the last chapter we saw that a uniform, dilute corona is thermally unstable towards infinitesimal perturbations. It was also shown that, for the specific cooling and heating functions adopted, the unstable mode does not reach equilibrium at a later stage for the range of the electron temperatures considered.

We now extend the analysis to non-linear perturbations and obtain the time scale of the condensation process out of the corona. It was postulated earlier that the condensation follows isobaric conditions. If the magnetic pressure is small, the matter density increases between initial and final stages by about a factor of 100, while the electron temperature falls by about the same factor. Observations indeed indicate that the internal gas pressure in the undisturbed corona is not too different from the gas pressure within prominences of the quiescent types. Such conditions for the equilibrium state of prominences were first suggested by Zanstra (1955a, 1955).

We also confine ourselves here to isobaric perturbations. Without much loss of generality we consider as a simplified model a cylindrical configuration within the corona, with a uniform magnetic field running parallel to the axis of the cylinder. Let the cylinder undergo radial compression due to some unknown disturbance. Thermal instability will set in and lead to further condensation according to the previous considerations. An increase in density enhances the cooling rate with the result that the temperature falls more than to compensate for the pressure

difference caused by the initial density increase. This leads to further condensation and the process continues until a final thermal equilibrium state is reached. In the present section we wish to follow the development of this condensation process.

The idea of isobaric perturbations is crucial in the present context. Since the medium is ionized, magnetic field lines are frozen in. This demands magnetic flux conservation during any change in the medium. Magnetic flux and mass conservation implies, for our specific model, that any increase in density causes a corresponding increase in the magnetic field strength; c.f. equation (2.14).

If during the transition from the corona to the prominence the density increases by a factor of 100, to compensate for the decrease in temperature and the final magnetic field would also have to be 100 times the original field strength. To insure isobaric conditions, the total pressure (magnetic plus gas pressure) must stay constant during the entire condensation process. This amounts to the requirement that the initial field should be of such a strength that it does not become large enough at any later stage to overcome the gas pressure. Thus, a prominence whose gas pressure exactly equals the coronal gas pressure can originate only in regions of very weak magnetic fields. For a coronal electron density of 10^8 cm^{-3} and an electron temperature of 1.5×10^6 ^oK, we have, assuming a final prominence temperature of 1.5×10^4 ^oK and an electron density of 10^{10} cm^{-3}, equality between magnetic pressure and gas pressure, if we start with 0.01 gauss. Hence, in order that the magnetic pressure may not dominate

in our specific mode of condensation, the initial magnetic field must be below 0.01 gauss. The corresponding final field would then be about 1 gauss. Such a value contradicts the observations by Zirin (1962) and more recent polarization studies by Hyder (1965) of quiescent prominences. The obvious conclusion seems to be that in general the gas pressure in the prominence should be somewhat less than the gas pressure in the surrounding corona.

One has to remember, however, that our model is highly idealized, in the sense, that it assumes either homogeneous plasmas or plasmas that are as close as possible to the homogeneous case. This idealization is probably quite appropriate in the early stages of the condensation, assuming the corona to be as unstructured as it is commonly suggested. Once the prominence has formed, however, it is obvious that aside from the already mentioned structurization rather violent, so-called "turbulent" motions set in that are well documented by Doppler studies. It is quite conceivable that by such processes magnetic field lines are entangled and transformed into bundles of relatively high strength. We feel that these things at present are not quite accessible to either theoretical or observational discussions.

Mass conservation requires that, if the density increases by a certain factor, the radius of the cylinder must decrease by the square root of this factor. The average observed overall thickness of a quiescent prominence is about 20,000 km. This means that the characteristic size of the condensation must be of the order of 200,000 km. It is interesting to note that observations by Williamson, Fullerton and Billings (1961) have

shown a lower density in the corona in the immediate neighborhood of quiescent prominences.

For such a scale length of 200,000 km, as has been shown in chapter 5 thermal conduction can be ignored. This simplifies the problem in the sense that one need not consider the spatial variation of the physical variables. Hence, we have only to solve the non-linear energy equation in order to follow the condensation process. The final equation to be integrated out is an equation in time only. Thus, the integration will supply us with the time scale for the evolution of a prominence.

As before the energy equation reads

$$\frac{dp_g}{dt} = \frac{5p_g}{3\rho}\frac{d\rho}{dt} + \frac{2}{3}\left[H(\rho,T_e) - E(\rho,T_e) + \vec{\nabla}\cdot(K_B\vec{\nabla}T_e)\right]. \qquad (6.1)$$

Upon ignoring thermal conduction equation (6.1) becomes

$$\frac{dp_g}{dt} = \frac{5p_g}{3\rho}\frac{d\rho}{dt} + \frac{2}{3}\left[H(\rho,T_e) - E(\rho,T_e)\right] . \qquad (6.2)$$

The condition of pressure equilibrium requires that

$$p_g + B^2/8\pi = p_g^o + B_o^2/8\pi \quad , \qquad (6.3)$$

where p_g and B are the values at any time, and p_g^o and B_o are the corresponding values at equilibrium.

Equations (6.2) and (6.3) can be written in the dimensionless form:

$$\frac{dy}{dt} = 2y[E(\rho,T_e) - H(\rho,T_e)]/5p_g^o[1+Z_o(1+0.20y^2)] \qquad (6.4)$$

and

$$p_g = p_g^o[1 + Z_o(1-y^2)] \ , \qquad (6.5)$$

where,

$$y = \rho/\rho_o \quad \text{and} \quad Z_o = B_o^2/8\pi p_g^o$$

Equation (6.5) expresses the temperature in terms of the density, viz.,

$$T/T_o = [1 + Z_o(1-y^2)]/y \ , \qquad (6.6)$$

Cooling and heating functions can now be expressed in terms of y. For the heating function we have

$$H = A_o\rho = (A_o\rho_o)\rho/\rho_o = A_1 y \ , \qquad (6.7)$$

and for the cooling function

$$E(\rho,T_e) = C_o\rho^2 f(T_e) = (C_o\rho^2/\rho_o^2)\rho_o^2 f(T_e) = C_o y^2 \rho_o^2 f(T_e) \ . \qquad (6.8)$$

Quantities with subscripts zero refer to equilibrium values. Equation (6.6) establishes a unique correspondence between temperature and density at any time. Using equation (6.6), we find for E the alternate form

$$E = y^2 \ N_{eo}'^2 \ G(y) \ , \qquad (6.9)$$

where,

$$N_e = N_e' \times 10^7$$

At equilibrium, we have $E_o = H_o$ and $y = y_o$. Thus the constant A_1 from equation (6.7) becomes

$$A_1 = y_o \, N'^2_{eo} \, G(y_o) \, . \qquad (6.10)$$

From equations (6.4), (6.9), and (6.10), we obtain the differential equation of our problem in the following form:

$$\frac{dy}{dt} = 2yN'^2_{eo} \, G(y_o)[y^2(G(y)/G(y_o))-y_o y]/5p^o_g[1+Z_o(1+0.20y^2)]. \qquad (6.11)$$

We first discuss the case of initial magnetic fields smaller than 0.01 gauss, where the product $N_e T_e$ stays essentially constant; c.f. section 5. We assume this product to have the value 1.05×10^{14} corresponding to an electron density of 7×10^7 at an electron temperature of 1.5×10^6 ^oK in the equilibrium stage. Defining a time constant t_o by

$$t_o = 5p^o_g/2N'^2_{eo} \, G(y_o) \text{ sec.}$$

we obtain

$$t_o = 7.24 \times 10^{-2}/G(y_o)N'^2_{eo} \, . \qquad (6.12)$$

Defining, further

$$\tau_o = 7 \, t_o \quad \text{and} \quad \tau = t/\tau_o \, , \qquad (6.13)$$

equation (6.11) reduces to

$$\frac{dy}{d\tau} = 7y[(y^2G(y)/G(y_o))-yy_o]/[1+Z_o(1+0.20y^2)] \qquad (6.14)$$

A perturbation of the medium may start from any equilibrium position. For instance, if $y_o = 1$, the corresponding temperature and density are 1.5×10^6 °K and 7×10^7, respectively. If $y_o = 2$, then $T_e = 7.5 \times 10^5$ °K and N_e is obtained from the constancy of the product $N_e T_e$.

Equation (6.14) was integrated numerically on an IBM 7094 computer. The Runge-Kutta scheme for numerical integration was followed. Since y has one to one correspondence with temperature through equation (6.6), we get a set of values for G(y) vs. y from the cooling curve. The function G(y) used above is indeed just the quantity E/N_e^2. From this set of values a table of G(y) vs. y was prepared such that the intermediate values could be obtained by linear interpolation. In the actual computation the cooling at any stage was read by the computer from the constructed table.

Two limiting values for the parameter Z_o, that contains the initial magnetic field, were chosen. The higher value corresponds to a field strength above which constant gas pressure cannot be preserved. The lower value corresponds to a field strength below which the magnetic field is no longer sufficient to inhibit thermal conduction across the field lines.

The integration was terminated when y reached a value of 60. This value corresponds to a temperature of 2.5×10^4 °K. At this stage a prominence has definitely formed.

In the actual computation our cooling curve, and Doherty and Menzel's results were used. The outcome is plotted as a graph of y vs. τ (Figs. 2 and 3). The value of τ at which the value of y increases sharply gives the characteristic time for prominence

evolution. These characteristic values τ_c and the corresponding times t_c in seconds are given in the Tables 7 and 8 for different equilibrium values. We have assumed in all these cases an initial disturbance of 2%. With larger disturbances the time scales become smaller. However, we feel that this parameter is of little importance. The tabulated values were computed for an initial coronal electron density of 7×10^7. For higher electron densities and the same temperature the time scale of condensation is correspondingly smaller.

In table 8, we have indicated the same value of τ_c for the two Z_o values, since the curves for these two values are practically coincident. The detailed computation of the stage where the "blow up" occurs shows that the condensation is slowed down somewhat at the higher field strength. Otherwise, however, the characteristic times are insensitive to the magnetic field strength so long as the latter neither moninates the volume pressure at any stage, nor permits a heat flow across the field lines. The numerical values of B_o, in terms of Z_o, as defined previously, are found from the relation

$$B_o^2 = 0.725\ Z_o \ . \qquad (6.15)$$

Thus, $Z_o = 5 \times 10^{-5}$ corresponds to a magnetic field of 6×10^{-3} gauss, whereas $Z_o = 5 \times 10^{-8}$ relates to a field of about 2×10^{-4} gauss.

We now turn to the situation where the magnetic field strengths are large enough to dominate over the gas pressure. Here again, we have integrated the non-linear equation (6.14) for initial

values of 0.12 gauss and 80 gauss. These fields correspond to Z_o values of 2×10^{-2} and 10^4, respectively.

Again keeping the perturbations isobaric, with an initial electron temperature of 1.5×10^6 °K and an electron density of 7×10^7 electrons/cm^3, equation (6.6) implies that for B_o = 0.12 gauss the temperature drops by a factor 50 while the density increases only by a factor of 6.7. The time scale for this process is 1.6×10^6 sec. at 2% perturbation in density. Thus, the final gas pressure is only about 10% of the coronal value, whereas the final magnetic field is at about 0.8 gauss.

For an initial field strength of about 80 gauss, we do not have any significant change in density, but the temperature drops by a factor of 50 when the density is perturbed by about 1 part in a 10^6. The time scale of the temperature collapse in this case is about 3×10^6 sec. This high field case corresponds to the incompressible case considered by Parker (1953). The evolution is displayed in Fig. 4.

The characteristic times as displayed in Tables 7 and 8 show clearly that the concept of thermal instability is able to provide a satisfactory explanation of prominence formation. We shall discuss in detail the conclusions to be drawn from our results in the next section, in particular, the limitations placed on the condensation process by magnetic fields and size considerations.

Time scale for prominence evolution using Doherty and Menzel's results.

Z_o = 5.00 x 10^{-8}, 2% perturbation in density.

Table 7.

y_o, equilibrium density	τ_c	$G(y_o)$	$7t_o$ sec.	$t_c=\tau_c x 7t_o$ sec.
1.00	0.111	$1.95x10^{-9}$	$5.30x10^{6}$	$5.88x10^{5}$
1.50	0.025	$5.89x10^{-9}$	$1.76x10^{6}$	$4.40x10^{4}$
2.00	0.015	$1.66x10^{-8}$	$6.23x10^{5}$	$9.35x10^{3}$
3.00	0.010	$5.89x10^{-8}$	$1.76x10^{5}$	$1.76x10^{3}$

Time scale for prominence evolution using the cooling function computed by us,

Z_o = 5.00 x 10^{-5}, 5.00 x 10^{-8}, 2% perturbation in density.

Table 8.

y_o, equilibrium density	τ_c	$G(y_o)$	$7t_o$ sec.	$t_c=\tau_c x 7t_o$ sec.
1.00	0.263	$1.74x10^{-9}$	$5.94x10^{6}$	$1.58x10^{6}$
1.50	0.060	$2.57x10^{-9}$	$4.03x10^{6}$	$2.40x10^{5}$
2.00	0.035	$4.36x10^{-9}$	$2.37x10^{6}$	$8.30x10^{4}$
3.00	0.011	$8.71x10^{-9}$	$1.19x10^{6}$	$1.30x10^{4}$

7. CONCLUSIONS

Our computations permit us to draw several important conclusions.

1. The mechanism of thermal instability is indeed able to describe at least the initial stages of the condensation of quiescent prominences out of the coronal medium. From our non-linear analysis, we find that the actual prominence state is reached after a time of typically 10^6 seconds. It would be interesting to compare continuous filtergrams of the type taken, for instance, at the Lockheed Solar Observatory for newly formed prominences. It may be possible to check the predicted formation times from this kind of observation.

2. The condensation mechanism requires the presence of magnetic fields, since in their absence thermal conduction by electrons would wash out immediately any developing temperature inhomogeneity. We found that at least a field strength of 10^{-4} gauss was necessary. On the other hand, magnetic fields exceeding about 10^{-1} gauss, though permitting drastic temperature decreases through thermal instability, result in a final matter density that remains the closer to the original coronal density, the higher the magnetic field strength is. Thus, the observation of prominences whose density is significantly above the density of the surrounding corona and which are permeated by magnetic fields of order 10 gauss require, after the initial drop in temperature, processes that cannot be understood in the framework of thermal instability.

3. The fact that most of the corona is not occupied by prominence-like material becomes a legitimate problem, since we

have shown that coronal material is unstable against any thermal instability across magnetic field lines. The most obvious explanation is due to the structure of the field which near the surface and outside of activity regions is nearly radial. Thermal instability is then simply prohibited by heat conduction along the quasi-radial field lines.

4. In the neighborhood of activity centers, however, the magnetic field should contain more or less closed structures that permit thermal instabilities to overcome conduction. It is significant that observations clearly show quiescent prominences to appear at the outskirts of spot groups, whereas the spot-related prominences of the loop-type appear as typically transient phenomena. One thus would conclude that quiescent prominences can form in connection with activity regions, due to their highly irregular field structures, but that for the same reason they are not able to develop into stationary phenomena right above the spot fields proper.

5. It would be interesting in the light of the foregoing discussion to compare records obtained from Babcock's magnetometer with the initial location of prominence formation. One might also look for a relation between the position of polar prominences and the transition region between the random fields at low and intermediate latitudes, and the more or less unipolar regions at high latitude.

APPENDIX A

The History of Observation

Prominences are localized phenomena in the solar corona. The earliest reference to prominences by observers dates as far back as the year 1842 [Ball (1893)]. It was not, however, until the eclipse of 1868 that the character of these objects, as really appertaining to the Sun, became properly understood. Janssen and Norman Lockyer, working independently, used the spectroscope for solar observations during this eclipse and demonstrated that the sun is surrounded by a more or less regular shell of gaseous matter, lying immediately outside the photosphere. Norman Lockyer gave the name "Chromosphere" to this outer layer, which at higher altitudes was thought to merge into the coronal medium.

In 1891, the invention of the spectroheliograph gave further impetus to the study of prominences. This new device, developed independently by Deslandres and Hale, enabled one to photograph the sun in different wavelengths. Further refinements in the observational techniques, after 1903, made it possible to follow prominences across the disk by means of their absorption of light from the chromosphere. They appeared as long dark ribbons superimposed on a bright background. Deslandres gave them the name "filaments," a name which is still in use today. Hale and Ellerman (1903) were the first to verify that the dark filaments appearing in spectroheliograms are nothing but prominences projected on the solar disk. These filaments when seen at the limb give the usual appearance of a bright prominence, like tongues of

flames colored by the intense emission in the H_{alpha} line of hydrogen.

In 1930, McMath incorporated motion picture techniques into the spectrum of observational methods. This innovation has proved to be of great value, especially in the observation of fast evolving phenomena such as surges, prominence disappearances, etc., and made it possible to study the complicated kinematics of prominence motion. The same year saw the invention of another powerful device called "coronagraph" by Lyot. This instrument finally enabled prominence research to forego the assistance of eclipses.

Classification

Prominences come in a variety of sizes and types. Even their place of origin in the solar atmosphere varies for different types. From the time of the very first observations, Father Secchi had noted two distinct classes, viz., eruptive and quiescent prominences. The words "eruptive" and "quiescent" are quite indicative of their dynamical aspects.

Pettit and McMath, with the help of modern techniques, refined the classification system into six major groups. Each major group was further subdivided into sub-groups. The major groups are the following: I. Active; II. Eruptive; III. Sunspot; IV. Tornado; V. Quiescent; VI. Coronal. Pettit's classification is based primarily on the form and character the prominences have at any time. One class may turn into another class during their evolution. Thus there is nothing physical about the classification,

useful as it is for taxonomic purposes.

Menzel and Evans (1953), from a detailed analysis of motion picture records, devised a "behavior" classification system of solar prominences. Two basic classes were recognized. In class A, luminous material primarily comes from above in the solar corona, whereas in class B, it originates from below in the chromosphere. Each class was further sub-divided into two sub-groups, namely, prominences associated with sunspots (S), and prominences not associated with sunspots (N). The final classification is as follows:

A. Prominences originating from above in coronal space.

S. Spot prominences: a. rain; b. funnels; l. loops.

N. Non-spot prominences: a. coronal rain; b. tree trunk; c. tree; d. hedgegrow; f. suspended cloud; m. mound.

B. Prominences originating from below in the chromosphere.

S. Spot prominences: s. surges; p. puffs.

N. Non-spot prominences: s. spicules.

The different names given by the authors convey a rough picture of the general appearances of prominences. Type A prominences are far more common than type B prominences.

In other schemes by Severny (1952) and by de Jager (Aller (1963)), motions and evolutionary histories serve as the essential basis of classification. It suffices to say that our model computations are aimed at understanding the origin of class AN in the above scheme by Menzel and Evans.

Distribution

The distribution of prominences on the solar disk is not uniform. They appear in two principal zones. The first group follows the sunspot zones, while the second group is confined to latitudes of about 45° at the start of a solar cycle, and migrates poleward. It reaches the pole near the maximum of solar activity and disappears soon after.

It is suggested that our discussion refers to prominences in the spot zones due to the close relation with magnetic fields. Too little is known on solar activity in polar regions to either include or exclude the polar prominences in our considerations.

Physical conditions

Prominences of Menzel and Evans's class A are dense and relatively cool objects embedded in the hot coronal medium, a fact demonstrated by the strong emission in the Balmer lines, the H and K lines of CaII , and lines of metals like FeI, FeII, MgII etc. Several workers have attempted to obtain values for the various physical parameters like electron density, kinetic temperatures of electrons and ions, "turbulent" velocity, etc., that are prevailing in a prominence.

To list a few papers we quote Athay and Orrall (1957), Jefferies and Orrall (1958, 1961a, 1961b, 1961c, 1962, 1963), Zirin and Tandberg-Hanssen (1960), Shih-Huei (1961), Hirayama (1963, 1964), Rigutti and Russo (1964), Tandberg-Hanssen (1964), and in addition the review articles by d'Azambuja (1948, 1955), Kiepenheuer (1953b), de Jager (1959), Menzel (1959), Menzel and Wolbach (1960,I,II).

Zirin and Tandberg-Hanssen (1960), in particular, compared spectra of active and quiescent prominences and stated that quiescent prominences display spectra similar to that of the chromosphere at 1500 km in their height scale with weak HeII lines, whereas, active prominences display broader lines and strong HeII lines. Broadness of lines was taken as indicative of higher internal motion within the prominence.

Recently Tandberg-Hanssen (1964) has studied the spectrum of a quiescent prominence in great detail and obtained absolute intensities for a large number of metal lines. The faintest lines quoted in his paper have intensities of $10^{-5} \times I_\lambda$, where I_λ is the specific intensity of the photospheric radiation at the particular wavelength. In the same paper the spectrum of a quiescent prominence is compared with that of a flare and of an active prominence. It is stated that for active prominences significant emissions are observed in the lines of Mg I λ 5523, HeII λ 5411, and the coronal line Ca XV λ 5445. On the other hand, the emission in the quiescent prominence is characterized by the lines of FeI, FeII, TiII, strongest of them all being the ScII lines, which, for instance, dominate completely the spectral region around 5600 Å.

The physical conditions within the prominence obviously exhibit large departures from thermodynamic equilibrium. The only meaningful measure of internal energy is the kinetic temperature of particles, assumed to be the same for electrons, ions, and atoms. The interpretation of spectra becomes all the more difficult when the temperature gradient in the transition region from the corona

to the prominence is taken into account. Deduced values of the kinetic temperature vary between 10^4 to 5×10^4 ^oK. A similarly large scatter exists for density values, ranging from 10^{10} to 10^{13} atoms per cm^3. Computed turbulent velocities lie in the range of 5 to 10 km sec. As a rule, higher temperatures and densities are found in AS prominences.

APPENDIX B

In defining our cooling function in Section 3, we stated that emission in subordinate metal lines as well as emission in subordinate hydrogen continua is negligible in comparison with emission in resonance lines. In support of this assertion, we would like to estimate in the following from published observational data, the relative importance of these line and continuum emissions for a quiescent prominence. Since the available measurements have only a partial overlap, we contracted all intensity values onto a common scale referring to an "average" quiescent prominence.

Balmer and Paschen emissions were obtained from a paper by Jefferies and Orrall (1961). For the lines due to hydrogen, helium and metal, intensity values in the range $\lambda\lambda$ 3600-3800 $\mathring{A}$ were taken from a paper by Jefferies and Orrall (1962). For the range $\lambda\lambda$ 3800-5896 $\mathring{A}$, Tandberg-Hanssen (1964) has given an extensive table of line intensities. Where no line intensities were given in the above references, we used the table of intensities published by Yakovkin and Zel'dina (1963).

Altogether the following intensities were found:

Balmer continuum emission at 3642 $\mathring{A}$ = 310 ergs $cm^{-2}sec^{-1}sterad^{-1}$ per $\mathring{A}$

Balmer continuum emission at 3672 $\mathring{A}$ = 55 " " " " "

Paschen continuum emission at 8200 $\mathring{A}$ = 108 " " " " "

Paschen continuum emission at 8367 $\mathring{A}$ = 72 " " " " "

Energy emitted by all metal lines in the

range $\lambda\lambda$ 3600-5900 $= 4.9 \times 10^5$ ergs $cm^{-2}sec^{-1}sterad^{-1}$

Energy emitted by Hydrogen lines $= 5.52 \times 10^5$ ergs $cm^{-2}sec^{-1}sterad^{-1}$

Energy emitted by Helium lines = 4.6×10^4 ergs $cm^{-2} sec^{-1} sterad^{-1}$

We now classify the metal lines into various intensity groups, (Table B.1). The strongest metal lines are tabulated separately (Table B.2). Most of these lines are resonance lines or lines from low lying levels. Hydrogen and Helium lines are also listed separately in Tables B.3 and B.4.

It is already quite obvious that the subordinate metal lines can never play a dominant part in the total emission of a volume element. In order to check the possibility that a large number of very faint lines below the observation threshold could shift the importance of subordinate lines by a significant amount, we have ordered the observed lines in groups according to their intensity. For instance, all lines with intensities between 20 and 40, between 40 and 80, between 80 and 160, ergs/cm^2/sec/sterad etc., were combined and their total emission determined. The results are shown in Fig. 5, where the logarithm of the total emission per class is plotted against the energy range on an essentially logarithmic scale. Actual results are represented by circles, the figures refer to the number of lines included in each count. The very strong resonance lines were left out as immaterial for the present purpose.

We have drawn a smooth curve through the points and continued it into the region of lower intensity. Admittedly, this extension is debatable in its detailed behavior. However, we feel that it is not too unreasonable if one recalls that the very weak lines are largely represented by transitions from higher excited states whose population under conditions of collisional excitation is

drastically reduced. From the extrapolation we find a total emission of less than 100 ergs/cm^2/sec/sterad in all weak lines. We can compare this estimate with the number of lines with intensities less than 20, listed in the observational data. This number comes to about 200, of which 90% have intensities less than 5. Even if each line had an intensity of 5, the total would still be completely negligible.

It thus seems to be quite permissible to neglect the emission of subordinate lines in the cooling function even at temperatures as low as some 10^4 ^oK which corresponds to the value quoted for an established quiescent prominence.

TABLE B.1

Intensity of metal lines in a quiescent prominence

Energy range in ergs $cm^{-2} sec^{-1} sterad^{-1}$	No. of lines in the energy range	Total energy in the lines in the range
20 - 40	6	180
40 - 60	6	300
60 - 80	6	420
80 - 100	10	900
100 - 120	8	880
120 - 140	9	1170
140 - 160	10	1500
160 - 180	9	1530
180 - 200	5	950
200 - 220	10	2100
220 - 240	7	1610
240 - 260	8	2000
260 - 280	7	1880
280 - 300	3	870
300 - 320	3	930
320 - 340	4	1320
340 - 360	2	700
360 - 380	3	1110
420 - 460	3	1320
460 - 500	2	960
500 - 540	4	2080
540 - 580	2	1120

TABLE B.1 (Continued)

Energy range in ergs $cm^{-2}sec^{-1}sterad^{-1}$	No. of lines in the energy range	Total energy in the lines in the range
700 - 740	1	720
740 - 780	4	3040
780 - 820	2	1600
820 - 860	1	840
900 - 940	3	2760
940 - 980	2	1920
980 - 1020	1	1000
1000 - 1400	6	7200
1400 - 1800	6	9600
1800 - 2200	3	6000
2200 - 2600	4	9600
2600 - 3000	3	8400
3000 - 3400	1	3200
3400 - 3800	1	3600
3800 - 4200	2	8000
4600 - 5000	2	9600
5000 - 5400	1	5200
5400 - 5800	1	5600
5800 - 6200	-	-
6200 - 6600	1	6400

Total energy contained in the metal lines listed above = 1.2×10^5 ergs $cm^{-2}sec^{-1}sterad^{-1}$

No. of faint lines within the energy range 4-20 ergs $cm^{-2}sec^{-1}sterad^{-1}$ = 200

Energy locked within these faint lines = 2×10^3 ergs $cm^{-2}sec^{-1}sterad^{-1}$

TABLE B.2

Intensity of very strong metal lines

Wavelength in Å	Atom	Energy in ergs cm^{-2} sec^{-1} $sterad^{-1}$	Remarks
3933.7	CaII	1.3×10^5	Resonance line
3968.5	CaII	1.2×10^5	Resonance line
4226.7	CaI	0.66×10^4	Resonance line
4077.7	SrII	1.5×10^4	Resonance line
4215.5	SrII	1.08×10^4	Resonance line
5167.2	MgI	1.6×10^4	$3^3P^o - 4^3S$
5172.7	MgI	1.8×10^4	$3^3P^o - 4^3S$
5183.6	MgI	3.3×10^4	$3^3P^o - 4^3S$
3838	MgI	1.0×10^4	$3^3P^o - 3^3D$
3832	MgI	8×10^3	$3^3P^o - 3^3D$

$3\ P^o$ is the next higher level from the ground state ^1S level.

Total energy contained in very strong lines = 3.69×10^5 ergs cm^{-2} sec^{-1} $sterad^{-1}$

Sodium D lines are included in Table B.1.

TABLE B.3

Hydrogen line intensities

Hydrogen line Transition to level 2 from level	λ in Å	Energy in ergs $cm^{-2} sec^{-1} sterad^{-1}$
3	6563	1.33×10^5
4	4861	1.56×10^5
5	4340	7.4×10^4
6	4102	6.0×10^4
7	3970	6.4×10^4
8	3889	2.4×10^4
9	3835	1.4×10^4
10	3798	7×10^3
11	3771	5×10^3
12	3750	3×10^3
13	3734	2×10^3
14	3722	1×10^3
15	3711.9	1×10^3
16	3703.8	1×10^3
17	3697.1	1×10^3
19	3686.8	9×10^2
20	3682.8	8×10^2
21	3679.3	7×10^2
22	3676.3	6×10^2
23	3673.7	5×10^2

TABLE B.3 (Continued)

Hydrogen line Transition to level 2 from level	λ in Å	Energy in ergs $cm^{-2}sec^{-1}sterad^{-1}$
24	3671.4	4×10^2
25	3669.4	3×10^2
26	3667.6	3×10^2

Total energy locked in Hydrogen lines given above =

$$5.52 \times 10^5 \text{ ergs } cm^{-2}sec^{-1}sterad^{-1}$$

TABLE B.4

Helium line intensities

λ in $\mathring{A}$	Energy in ergs $cm^{-2}sec^{-1}sterad^{-1}$	Remarks
3732.86	33	
3732.4	33	
3705.0	158	
3705.4	158	
3634.27	95	
3634.37	95	
3888.6	1.13×10^4	$2^3S - 3^3P^o$
4026.2	2.54×10^3	
4121.0	2×10^2	
4387.9	3×10^2	
4471.5	1.89×10^4	$2^3P^o - 4^3D$
4713.2	2.2×10^3	
5875.6	1.08×10^4	$2^3P^o - 3^3D$

Total energy locked in Helium lines given above

$$= 4.6 \times 10^4 \text{ ergs } cm^{-2}sec^{-1}sterad^{-1}$$

APPENDIX C

In section 5, thermal conduction was ignored as an energy gain mechanism in comparison with radiative cooling.

To justify this procedure for our models that are dealing with very small magnetic fields, we compare in Table C.1 cooling due to radiation and heating due to thermal conduction across magnetic field lines. The isobaric condition, that is, constancy of total pressure implies constancy of gas pressure, or

$$\varphi = N_e T_e \text{ (constant)}$$

We choose a value of 1.05×10^{14} for φ that follows from $N_e = 7 \times 10^7$ and $T_e = 1.5 \times 10^6$ ^oK. The radiative losses quoted have been obtained from our computation.

In the presence of a magnetic field the thermal conductivity across the lines is reduced by a factor $(\omega_e^2 t_e^2)^{-1}$ if $\omega_e^2 t_e^2 \gg 1$, where ω_e is the electron cyclotron frequency, t_e is the mean time between collision. The remaining momentum transfer is mainly due to ions. If, on the other hand, $\omega_e^2 t_e^2$ is of the order of unity or below, the conduction is due to electrons. For our case of $\omega_e^2 t_e^2 \gg 1$, the coefficient of thermal conductivity is given by

$$K_o = 6 \times 10^{-17} \varphi^2 B^{-2} T_e^{-5/2} \text{ ergs deg}^{-1}\text{sec}^{-1}\text{cm}^{-1} .$$

K_o can be written as

$$K_o = 6 \times 10^{-6} T_e^{5/2} / \omega_e^2 t_e^2$$

TABLE C.1

T_e in ^oK	B in gauss	E, radiative cooling in ergs/cm^3/sec (Raju)	$4\pi^2 K_o T_o \lambda_o^{-2}$	$\omega_e^2 t_e^2$
1.5×10^6	10^{-4}	8.54×10^{-8}	$1.45\times10^{12}\lambda_o^{-2}$	7.6×10^5
1.0×10^6	1.5×10^{-4}	2.82×10^{-7}	$1.16\times10^{12}\lambda_o^{-2}$	2.25×10^5
4.0×10^5	3.75×10^{-4}	9.94×10^{-6}	$7.25\times10^{11}\lambda_o^{-2}$	1.44×10^4
1.0×10^5	1.5×10^{-3}	7.77×10^{-4}	$3.67\times10^{11}\lambda_o^{-2}$	2.25×10^2
4.0×10^4	3.75×10^{-3}	1.39×10^{-3}	$2.31\times10^{11}\lambda_o^{-2}$	1.44×10

with,

$$\omega_e^2 t_e^2 = 10^{11}\, B^2 \varphi^{-2} T_e^5$$

It is clear that one can ignore thermal conduction if $K_o T_e k^2$ is less than the radiative cooling rate, where

$$k = 2\pi/\lambda_o$$

is the wave number of the disturbance. We thus have to compare $4\pi^2 K_o T_e/\lambda_o^2$ with the radiative loss. The remaining problem is the selection of appropriate k- or λ_o-values.

To reach the prominence state, N_e must increase by about a factor of 100, with the kinetic temperature decreasing by about the same factor. We choose the initial field to be 10^{-4} gauss. Since the field is frozen in, the later values are given by the condition

$$B_{initial}/B = N_{e\ initial}/N_e$$

For a cylindrical model with radial condensation, the radius would have to decrease by the square root of the condensation factor. If the final prominence diameter is 20,000 km, then the initial scale length of the disturbance must be 200,000 km.

For this given initial field, and a scale length of 200,000 km we see from the table that we indeed can ignore thermal conduction. One also sees that as the condensation proceeds conduction can be ignored with even much smaller values for λ_o. This remark is important if we recall that an actual prominence is made up of filamentary structures of relatively small diameter. While at

4×10^4 °K the overall scale length would be around 33,000 km λ_o-values as small as 1000 km would still be permissible.

If we start with fields much lower than 10^{-4} gauss, then the initial scale length for a disturbance becomes too large to be acceptable on observational grounds, in addition to the fact that the necessary inhibition of electron conduction is lost; c.f. below. If we vary B and φ (which means varying N_e) in such a way that $B^2\varphi^{-2}$ remains constant, we see that 10^{-4} gauss indeed is the lower limit of acceptable field strengths.

We conclude this discussion of thermal conduction by showing in a qualitative sense that it is vital to inhibit electron conduction both during the formation of a prominence, and after it is in stationary state. In fact, thermal conduction in the absence of a magnetic field would heat up a prominence in a matter of minutes. A detailed calculation on this subject was carried out by Tandberg-Hanssen, Jensen and Rosseland (1958).

Heating by thermal conduction is governed by the diffusion equation,

$$C \frac{\partial T_e}{\partial t} = \frac{\partial}{\partial x} \left(K \frac{\partial T_e}{\partial x} \right) \quad . \qquad (C.1)$$

The coefficient of thermal conduction in the absence of a magnetic field is (Orrall and Zirker (1961))

$$K = 3 \times 10^{-6} \, T_e^{+5/2}$$

C is the specific heat per unit volume, viz.,

$$C = 5N_e k$$

x is the co-ordinate across the transition region over which the temperature falls from the coronal to the prominence value.

Using the expression for K in equation (C.1), we get

$$C \frac{\partial T_e}{\partial t} = 3 \times 10^{-6}\left[\frac{5}{2} T_e^{3/2} \left(\frac{\partial T_e}{\partial x}\right)^2 + T_e^{5/2} \frac{\partial^2 T_e}{\partial x^2}\right] \qquad (C.2)$$

For an estimate of orders of magnitudes, the differentials may be replaced by differences, viz.,

$$C \frac{\Delta T_e}{\Delta t} \approx \frac{15}{2} \times 10^{-6} T_e^{3/2} \frac{(\Delta T_e)^2}{(\Delta x)^2} \qquad (C.3)$$

$\Delta t = t_c$ is now the characteristic time for the heating process, $\Delta x = \ell$ the scale length of the transition region. Taking $\Delta T_e = T_e$, we obtain

$$t_c = (2/3) \times 10^6 \ell^2 N_e k T_e^{-5/2} \qquad (C.4)$$

choosing $N_e = 10^9$ cm^{-3} and $T_e = 10^6$ °K, we find

$$t_c = 9.2 \times 10^{-17} \ell^2 \qquad (C.5)$$

Some typical numerical values for t_c are given below in Table C.2 as a function of the transition length ℓ.

The table clearly shows that the characteristic times are not only negligibly small in comparison with the observed life-times of quiescent prominences for any reasonable value of ℓ, but also with the formation times derived in this paper.

To overcome conduction one thus needs the postulated magnetic fields.

TABLE C.2

ℓ in km	t_c in sec
10	9.2×10^{-5}
100	9.2×10^{-3}
1000	9.2×10^{-1}
10,000	92

REFERENCES

Allen, C. W. 1963, Astrophysical Quantities (2d ed.; London: University of London, Athlone Press), p. 43.

Aller, L. H. 1963, The Atmospheres of the Sun and Stars (New York: Ronald Press).

Athay, R. G., and Orrall, F. Q. 1957, Ap. J. 126, 167.

Azambuja, M. and L. d', 1948, Ann. Obs. Paris, Meudon, Vol. 6, Fasc. VII.

d'Azambuja, L. 1955, Vistas in Astronomy, Vol. I, 695.

Ball, R. 1893, The Story of the Sun (Cassell and Co, Ltd.), p. 173.

Doherty, L. R., and Menzel, D. H., 1965, Ap. J., 141, 251.

Dungey, J. W. 1953, M.N., 113, 180.

Elwert, G. 1954, Zs. f. Naturforschung, 9a, 637.

Field, G. B. 1965, Ap. J., 142, 531.

Hale, G. E., and Ellerman, F. 1903, Pub. Yerkes Obs., 3, Part I, 3.

Hirayama, T. 1963, Publ. A.S. Japan, 15, 277.

_____ 1964, ibid, 16, 104.

House, L. 1964, Ap. J. Suppl, 8, 307.

Hunter, J. H. 1966, Icarus, in press.

Hyder, C. L. 1965, Ap. J., 141, 1374.

Ivanov-Holodnyi, G. S., and Nikolskij, G. M. 1961, Soviet AJ, 5, 31.

_____, ibid, 5, 632.

Jager, C. de. 1959, Hd. d. Physik, Vol. 52, 224.

Jefferies, J. T., and Orrall, F. Q., 1958, Ap. J., 127, 714.

_____ 1961a, ibid, 133, 946.

_____ 1961b, ibid, 133, 963.

_____ 1961c, ibid, 134, 747.

_____ 1962, ibid, 135, 109.

_____ 1963, ibid, 137, 123.

Kiepenheuer, K. O. 1953a, Convegno volta, 11, Roma, 148.

_____ 1953b, The Sun, ed. G. P. Kuiper (Chicago: University of Chicago Press), Chap. vi, p. 394.

_____ 1959, Zs. f. Ap., 48, 290.

Kippenhahn, R., and Schlüter, A. 1957, Zs. f. Ap., 43, 36.

Kleczek, J. 1957, Bull. Astr. Inst. Czechoslavokia, 8, 120.

_____ 1958, ibid, 9, 115.

Lüst, R., and Zirin, H. 1960, Zs. f. Ap., 49, 8.

Menzel, D. H. 1951, Report on conference on the Dynamics of Ionized Media, London, 1951.

Menzel, D. H., and Evans, D. S. 1953, Convegno volta, 11, 119.

Menzel, D. H. 1959, Our Sun (Harvard University Press).

Menzel, D. H., and Wolbach, J. G. 1960 Sky and Telescope, Vol. 20 I, 252; II, 330.

Orrall, F. Q., and Zirker, J. B. 1961, Ap. J., 134, 72.

Oster, L., and Sofia, S. 1966, Ap. J., 143, 944.

Parker, E. N. 1953, Ap. J., 117, 431.

Pottasch, S. R. 1965, B.A.N., Vol. 18, 7.

Rigutti, M., and Russo, D. 1964, Zs. f. Ap., 58, 153.

Severny, A. B. 1952, Dokl. Akad. Nauk SSSR, 82, 25.

Shih-Huei, Y. 1961, Izv. Krimsk, Ap. Obs, 25, 180.

Tandberg-Hanssen, E. 1964, Astrophysica Norvegica, Vol IX, 14.

Tandberg-Hanssen, E., Jensen, E., and Rosseland, S. 1958 I.A.U. Symposium, No. 6, p. 150.

Uchida, Y. 1963, Publ. Astr. Soc. Japan, 15, 65.

Varsavsky, C. M. 1961, Ap. J. Suppl., 6, 75.

Weymann, R. 1960a, Ap. J., 132, 380.

_____, 1960b, ibid., 132, 452.

Williamson, N. K., Fullerton, C. M., and Billings, D. E. 1961, Ap. J., 133, 973.

Yakovkin, N. A., and Zel'dina 1963, Soviet AJ, 7, 643.

Zanstra, H. 1955a, Gas Dynamics of Cosmic Clouds, ed. L. Woltzer (New York: W. A. Benjamin, Inc.).

_____ 1955 , Vistas in Astronomy, 1, ed. A. Beer (New York: Pergamen Press).

Zirin, H., and Tandberg-Hanssen, E. 1960, Ap. J., 131, 717.

Zirin, H. 1962, Soviet AJ., 5, 660.

Figure 1.

A plot of log $(E/N_e'^2)$ versus log of electron temperature. E is the total radiative cooling rate in ergs/sec/cm^3 and N_e' is considered to be a pure number.

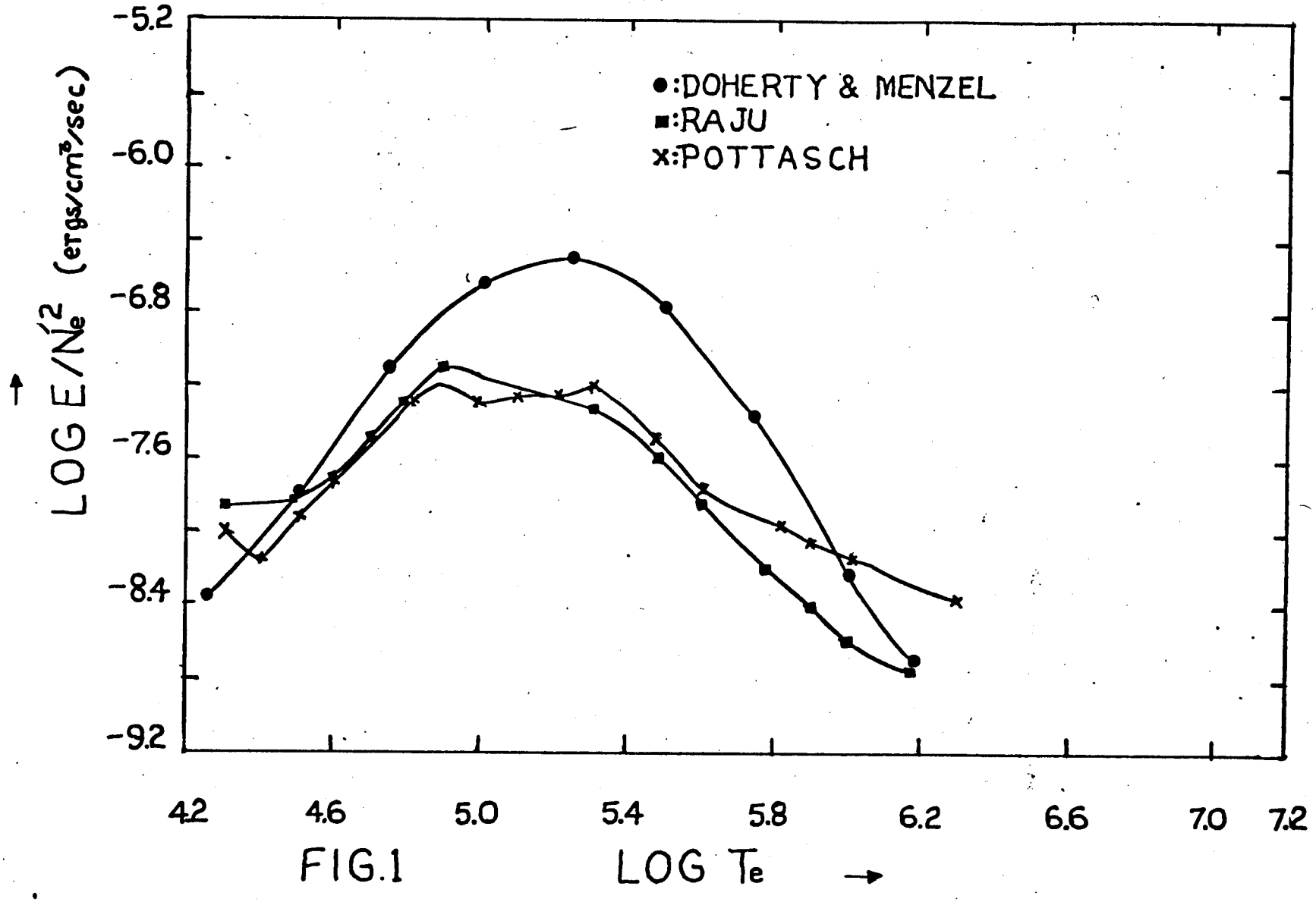
-5.2
-6.0
-6.8
-7.6
-8.4
-9.2
LOG E/Ne2 (ergs/cm3/sec)
●:DOHERTY & MENZEL
■:RAJU
x:POTTASCH
4.2
4.6
5.0
5.4
5.8
6.2
6.6
7.0
7.2
LOG Te

FIG.1

Figures 2 and 3.

Plots of dimensionless density parameter y ($= \rho/\rho_o$) versus dimensionless time parameter τ ($= t/\tau_o$). ρ is the initial equilibrium density in gm/cm^3. τ_o is some time constant in seconds defined in the text. The curves correspond to the cooling functions computed by Raju, and Doherty and Menzel. The equilibrium density values have been perturbed by 2%. We indicate one curve wherein perturbation in density is 10%. A value of y at any time has a corresponding value of temperature given by the equation (6.6) in the text. The curves for the two different values of Z_o ($= B_o^2/8\pi p_g^o$), corresponding to field strengths of 2×10^{-4} and 6×10^{-3} gauss, are the same. The dotted curve corresponds to the field strength of 0.12 gauss. For the dotted curve the value of $y = 6.66$ corresponds to a temperature of 30,000 ^oK, if the unperturbed equilibrium value of y is 1.

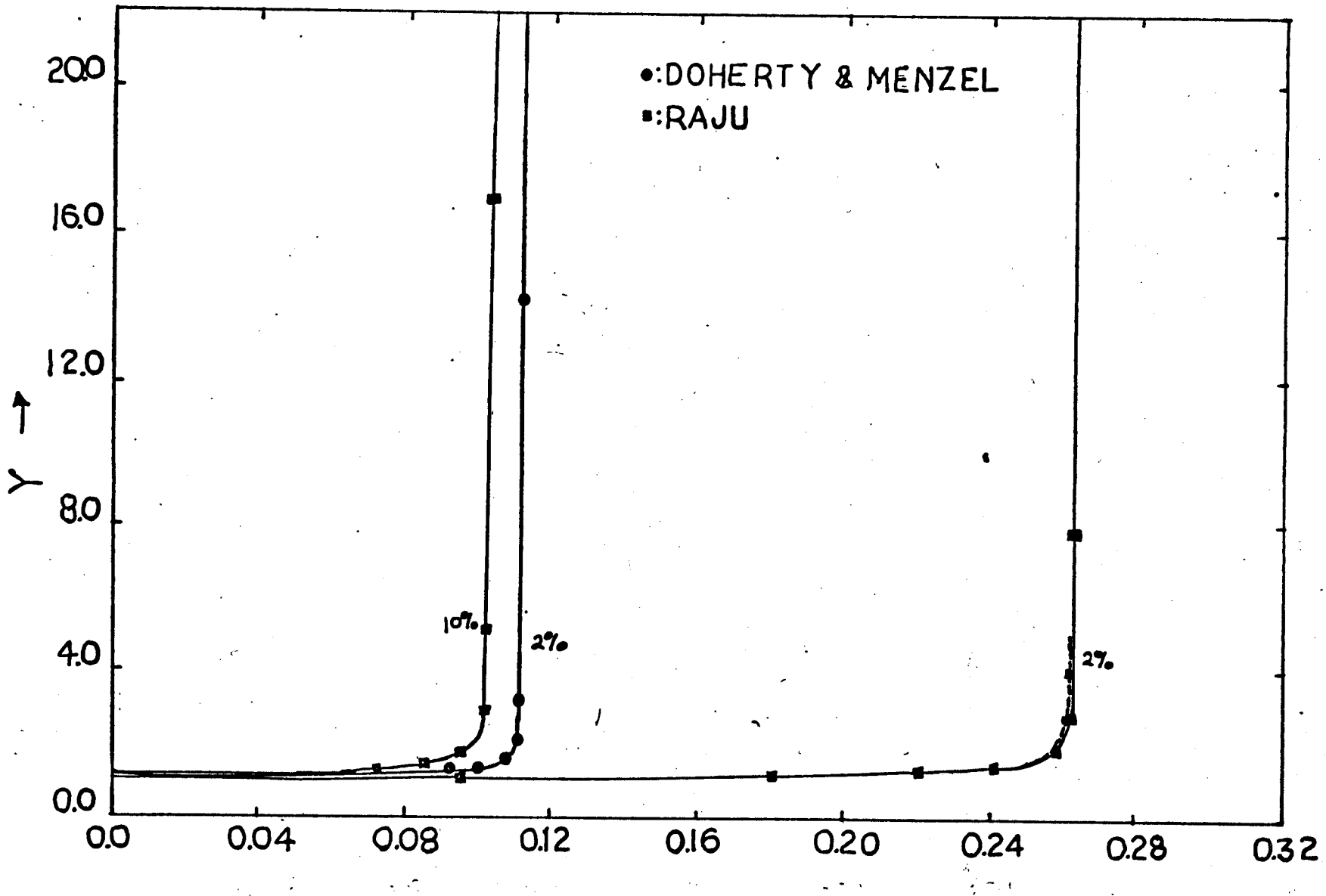
●:DOHERTY & MENZEL
▪:RAJU
20.0
16.0
12.0
8.0
4.0
0.0
Y
0.0
0.04
0.08
0.12
0.16
0.20
0.24
0.28
0.32
τ
1%
2%
2%

FIG. 2

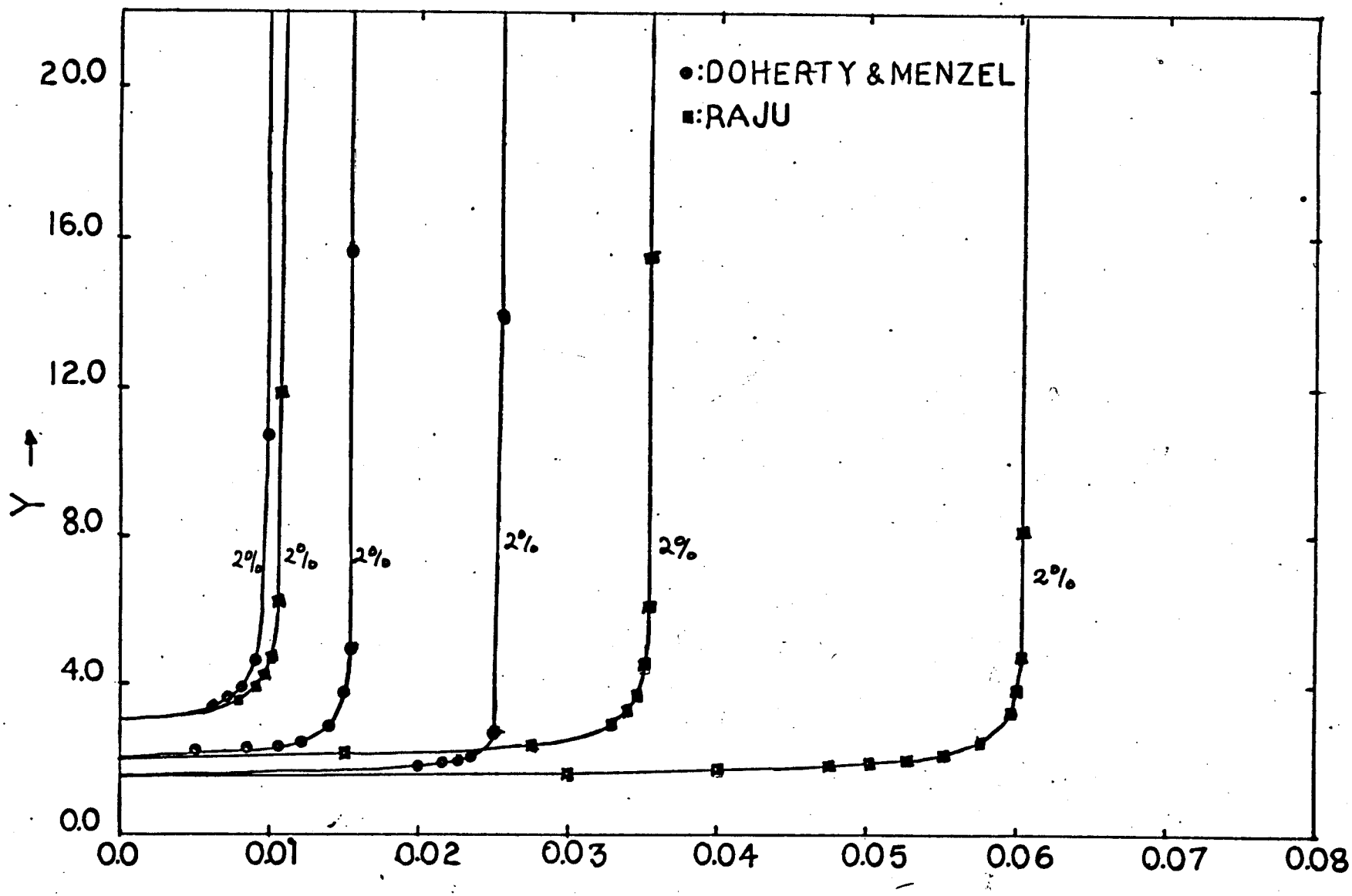
●:DOHERTY & MENZEL
■:RAJU
20.0
16.0
12.0
8.0
4.0
0.0
Y
2%
2%
2%
2%
2%
2%
0.0
0.01
0.02
0.03
0.04
0.05
0.06
0.07
0.08
τ

FIG. 3

Figure 4.

A plot of the change in dimensionless density parameter y ($= \rho/\rho_o$) versue the dimensionless time parameter τ ($= t/\tau_o$). τ_o is some time constant defined in the text. Radiative cooling rate adopted for this plot is the one computed by Raju. The equilibrium value of y is chosen to be 1. This value of y has been perturbed initially by one part in a million. The equilibrium magnetic field strength is about 80 gauss. For a given value of y at any time the corresponding temperature is given by the equation (6.6) in the text. The value of $y = 1{,}000{,}049$ corresponds to a temperature of 30,000 ^{o}K, if the initial temperature is 1.5×10^{6} ^{o}K and the electron density is 7×10^{7} electrons/cm^{3}.

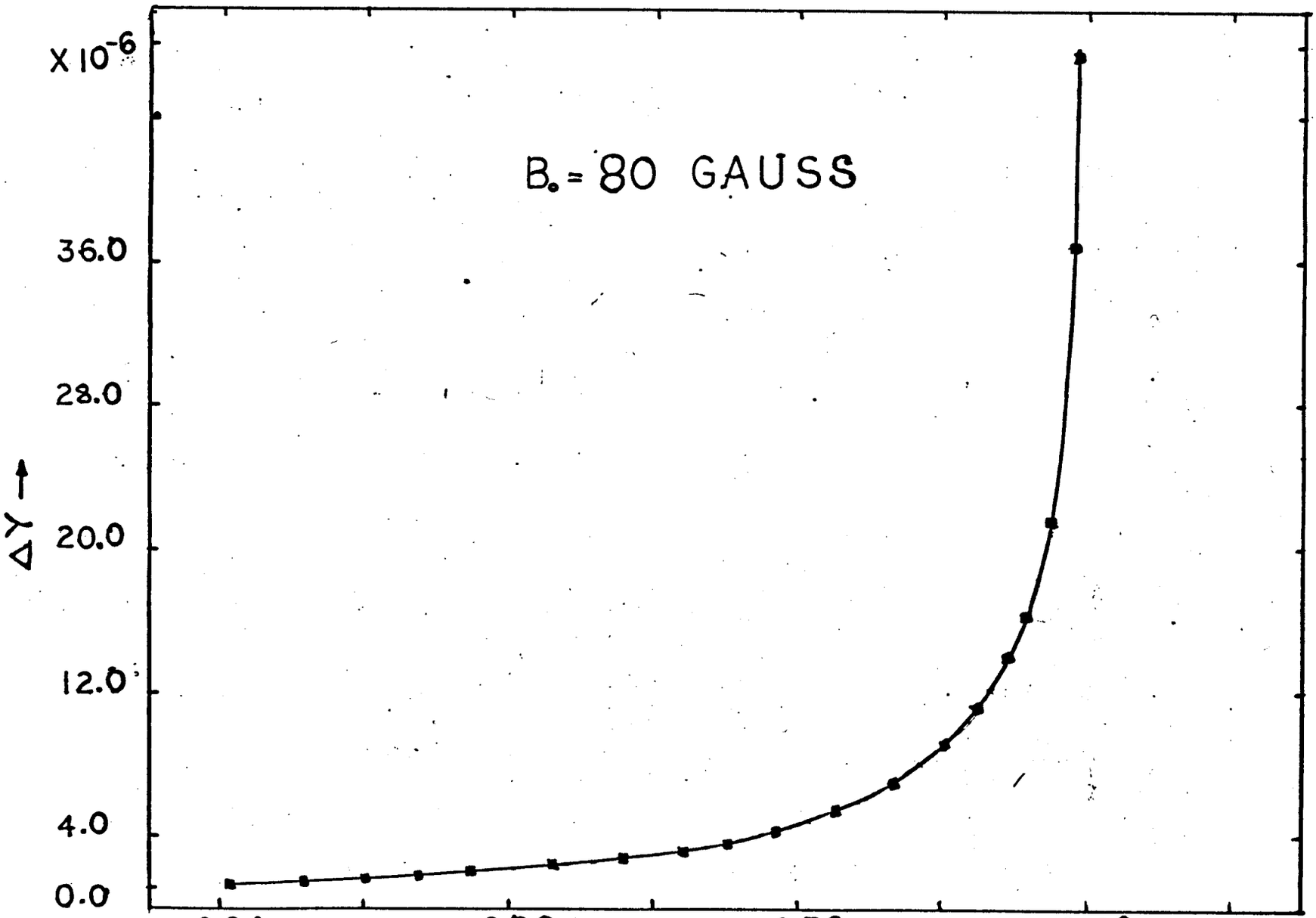

FIG. 4

Figure 5.

A plot of the logarithm of the total emission in ergs/cm^2/sec/sterad, per class against the energy range on an essentially logarithmic scale. The actual results are represented by circles, the figures refer to the number of lines included in each count. The very strong resonance lines were left out as immaterial for the present purpose.

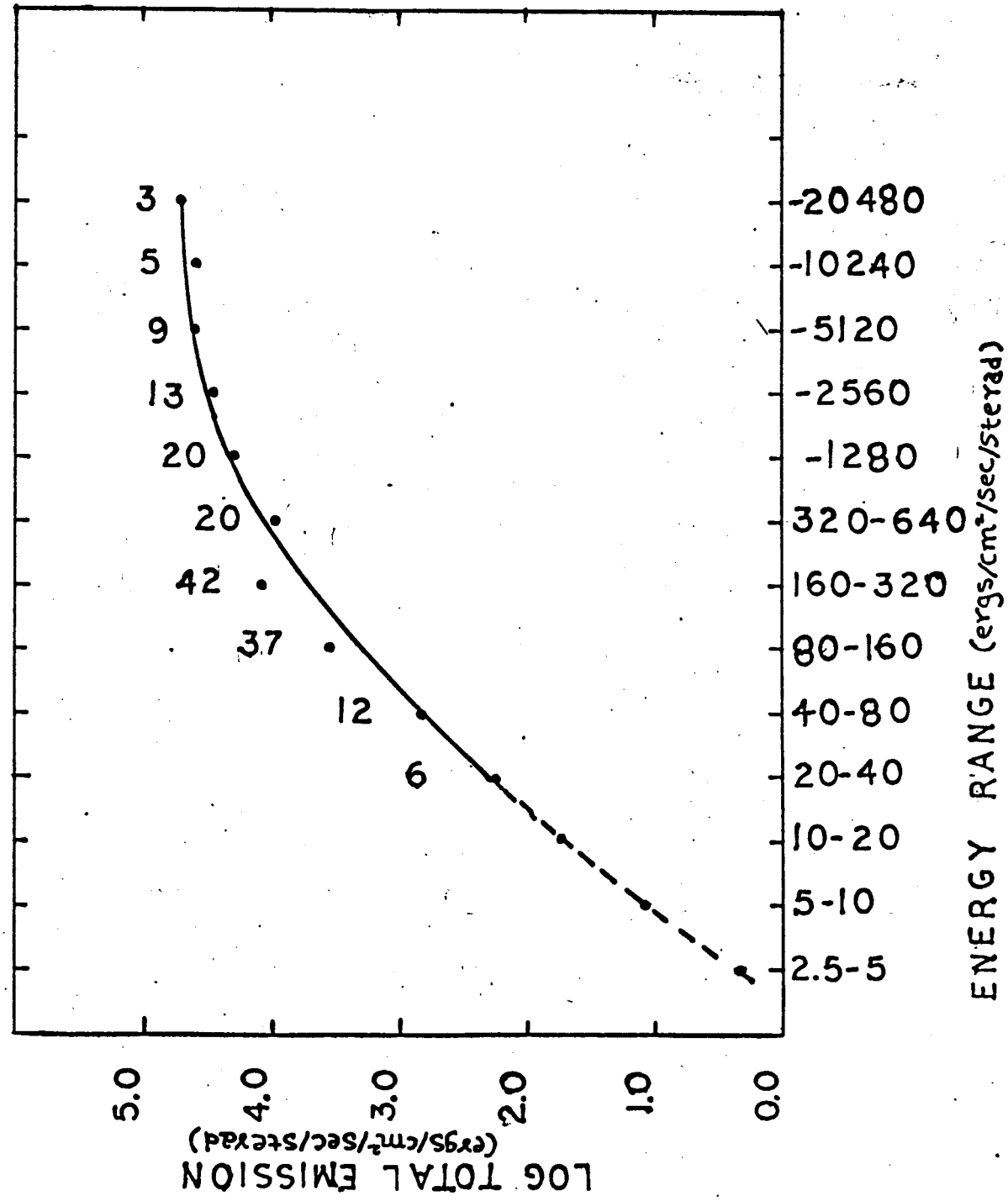
3
5
9
13
20
20
42
37
12
6
-20480
-10240
-5120
-2560
-1280
320-640
160-320
80-160
40-80
20-40
10-20
5-10
2.5-5
ENERGY RANGE (ergs/cm²/sec/sterad)
5.0
4.0
3.0
2.0
1.0
0.0
LOG TOTAL EMISSION
(ergs/cm²/sec/sterad)

FIG. 5